Distribution Agreement

In presenting this thesis as a partial fulfillment of the requirements for a degree from Emory University, I hereby grant to Emory University and its agents the non-exclusive license to archive, make accessible, and display my thesis in whole or in part in all forms of media, now or hereafter now, including display on the World Wide Web. I understand that I may select some access restrictions as part of the online submission of this thesis. I retain all ownership rights to the copyright of the thesis. I also retain the right to use in future works (such as articles or books) all or part of this thesis.

Bakai Sheyitov April 10, 2023

Establishing kinetic activity of Exonuclease III

on surface-immobilized substrates used in novel DNA rolling motors

By

Bakai Sheyitov

Khalid Salaita
Adviser

Chemistry

Khalid Salaita

Adviser

Brian Dyer

Committee Member

Antonio Brathwaite

Committee Member

2023

Establishing kinetic activity of Exonuclease III

on surface-immobilized substrates used in novel DNA rolling motors

By

Bakai Sheyitov

Khalid Salaita

Adviser

An abstract of a thesis submitted to the Faculty of Emory College of Arts and Sciences
of Emory University in partial fulfillment
of the requirements of the degree of
Bachelor of Science with Honors

Chemistry

2023

Abstract

Establishing kinetic activity of Exonuclease III

on surface-immobilized substrates used in novel DNA rolling motors

By Bakai Sheyitov

The kinetic capabilities of the enzymes used in nanotechnology, including in molecular motors, are often overlooked and poorly defined. This study aims to investigate the kinetic and biophysical profile of Exonuclease III, a common 3'-to-5' dsDNA exonuclease, and find its cleavage rate of two types of DNA substrates: freely floating in solution and immobilized on the surface. Comparing the hydrolysis rates in two environments allowed us to draw conclusions about Exonuclease III's kinetic activity and potential use in creating synthetic motors, specifically rolling motors. The rolling motor is a design in which the enzyme consumption of the nucleic acid monolayer propels the super-diffusive motion of the particle with multivalent DNA legs. An earlier generation of motors used RNase H hydrolysis of the RNA monolayer to power such motion. This work focuses on applying the findings from in-solution and on-surface kinetic assays to optimization of the design of RNA-independent rolling nanomotors. Our results show that Exonuclease III is capable of processive cleavage of DNA substrates in both conditions with in-solution k_{cat} of 12.8 min^{-1}, on-surface k_{cat} of 0.1-0.3 min^{-1}, and on-surface k_{off} of 0.1-0.2 min^{-1} when 8 nM ExoIII was added to the buffer containing 10 mM of Mg^{2+}. Additionally, the ability of certain protecting groups and fluorophores to affect the enzymatic cleavage was tested. A closer look at the Exonuclease III's behavior in various conditions and with substrates in distinct biophysical settings (in solution and on surface) addressed the fundamental questions of enzyme kinetics and laid a foundation for engineering a new class of nucleic acid-based molecular motors.

Establishing kinetic activity of Exonuclease III

on surface-immobilized substrates used in novel DNA rolling motors

By

Bakai Sheyitov

Khalid Salaita

Adviser

A thesis submitted to the Faculty of Emory College of Arts and Sciences
of Emory University in partial fulfillment
of the requirements of the degree of
Bachelor of Science with Honors

Chemistry

2023

Acknowledgements

I would like to express my gratitude to Dr. Khalid Salaita for his guidance and support throughout my academic and research journey at Emory University. I have known Khalid since the very first week of classes when he gave me a tour of the department as my pre-major adviser. From that day and on, I have grown fascinated with his expertise, energy, and enthusiasm. As a research adviser, Dr. Salaita provided a highly-supportive and flexible framework that allowed me to pursue independent undergraduate research in the interdisciplinary and innovative field of DNA nanotechnology and biophysics. Dr. Salaita's contribution to my future in the graduate school and beyond truly cannot be overstated.

I would also like to thank Yusha Imtiaz, my graduate mentor, who has done a great job introducing me to both the theoretical and tangible sides of research. Through our day-to-day interactions with Yusha, I have gained fundamental knowledge of molecular motors and enzyme kinetics as well as learned transferable skills of effective experimentation, analysis, and communication of my work. Outside the lab, Yusha has actively encouraged me to stay positive and prioritize my health and well-being – indeed, crucial factors for success in science.

I thank Dr. Brian Dyer and Dr. Antonio Brathwaite for serving on my thesis committee and providing feedback on my research progress. Both Dr. Dyer and Dr. Brathwaite have taught me important chemistry, biology, and physics topics through classes and conversations, as well as supported advancements in my academic career.

A big thank you goes to the Salaita research group! We are a big, diverse, and loud community of driven scientists, and I am honored to work alongside each and every one in our lab. I would like to acknowledge my rolling motors subgroup, Hiroaki Ogasawara, Selma Piranej, Krista Jackson, Luona Zhang, and Tianyi Zhang, for helpful feedback and discussion of my work. Other lab members, including Jhordan Rogers, Joseph Mancuso, Mohamed Husaini Bin Abdul Rahman, Tharindu Rajasooriya, and Steven Narum, have given advice and/or contributed to the completion of this and other experiments and projects.

I am also very proud to be a member of the larger Emory community. A network of peers and professors, mentors and mentees, supervisors and supporters, skeptics and cheerleaders that I encountered in college significantly shaped my personal and professional trajectory and prepared me for challenges and opportunities ahead. Per our motto, as *the wise heart seeks knowledge*, I am ready to seek further knowledge and grateful for everyone who has supported my feat.

Table of Contents

Background

Natural enzymes are abundant metabolic agents that accelerate biochemical reactions and are involved in various physiological functions of the cell, from signal transduction[1] to respiration[2] to DNA replication[3]. Apart from a few notable exceptions, such as RNA enzymes known as ribozymes[4], biological enzymes are protein structures with high specificity and defined catalytic activity. Broadly speaking, enzymes are classified by the reaction they catalyze: as such, oxidation or reduction is facilitated by oxidoreductases[5], while isomerases[6] take part in the bond rearrangement, or in other words, isomerization. Another noteworthy class of biological enzymes is hydrolases[7], enzymes responsible for the hydrolytic cleavage of bonds of varied biomolecular substrates: proteins (proteases[8]), lipids (lipases[9]), polysaccharides (glycoside hydrolases[10]), and nucleic acids (nucleases[11]).

Nucleases are phosphodiesterases that cleave the P-O bonds of nucleic acids and thus degrade longer polynucleotide chains into smaller oligonucleotide units.[12] Fundamentally, nucleases are enzymes employed in the bimolecular substitution of either 5' or 3' of a scissile phosphate using water as a common nucleophile (**Fig. 1**).[12] The primary roles of nucleases in the cell are DNA replication[13] and repair[13]; however, nucleases play important role in vital cellular processes such as site-specific recombination[14], topoisomerization[15], cell death[16] and RNA splicing[17].

A common precedent in the current literature is to divide protein nucleases into exo- and endonucleases based on their interaction with the DNA or RNA polynucleotide chain:

exonucleases cleave the chain from its ends, while endonucleases begin the hydrolysis of phosphodiester bonds within the inner sites of substrate strands. Classification of nucleases could also stem from the enzyme's ability to cleave either DNA (DNases) or RNA (RNases). It is important to note that it is often difficult to make a distinct division of a nuclease into the classes mentioned above – many enzymes possess dual activities and engage with nucleic acids more complexly.[18]

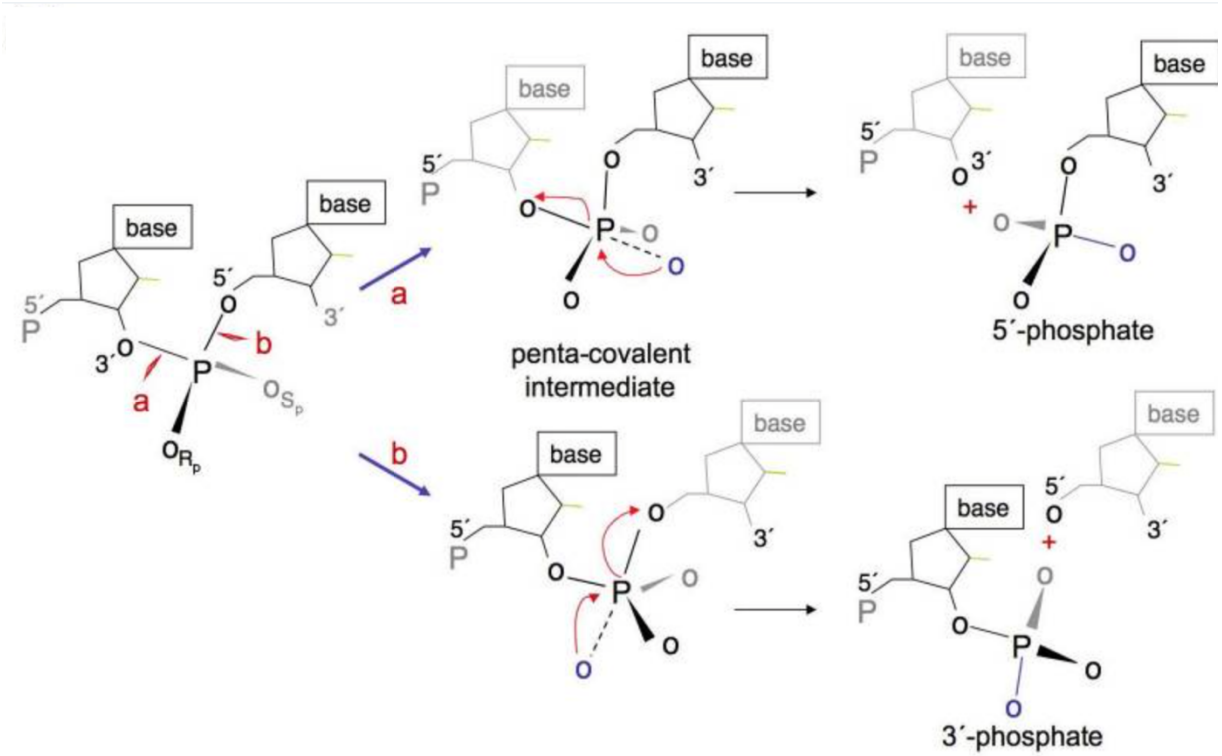

Figure 1. DNA cleavage by the nuclease.[12] *Two routes of the reaction mechanism of the nuclease hydrolyzing the DNA phosphodiester bond produce either 3' or 5' phosphate products. Reproduced from Reference 12 (CC BY-NC 3.0).*

Current literature suggests that there are 17 exonucleases reported in *E.coli,* including DNA polymerases, 3' to 5' and 5' to 3' exonucleases, Rec exonucleases, exo/endonucleases, as well as exonucleic activities of RNase T and endonucleases.[12,18,19] The respective functionality of the enzyme is dependent on its intrinsic properties and mechanism of action. The defining characteristics of exonucleases are substrate specificity, polarity of degradation, the type of reaction products, and processivity (**Table 1**). Most exonucleases are specific in their ability to cleavage strictly DNA or RNA; however, a small number of enzymes, such as RNase T have a unique capability to hydrolyze both DNA and RNA substrates.[20] The division based on the activity on either ssDNA or dsDNA is more ambivalent: some enzymes interact only with ssDNA (ExoI) or only with dsDNA (T7 Exo) or both (ExoV, DNase I).[12] Exonucleases are also split into two groups based on the polarity or direction they hydrolyze the polynucleotide chain: from 5' to 3' (T7 Exo) or from 3' to 5' (ExoIII, ExoI).[19,21,22] Products generated from exonuclease activity range from single deoxyribonucleoside monophosphates to short oligos to ssDNA. Processivity, or the ability of exonuclease to remain associated with the polynucleotide and continue its cleavage, is another critical factor distinguishing various exonucleases from each other.[23]

Table 1. Selected enzymes and their properties.[25]

Enzyme	Specificity	Polarity	Cleavage products
ExoIII	dsDNA	3’ → 5’	dNMPs, ssDNA
ExoI	ssDNA	3’ → 5’	dNMPs
T7 Exo	dsDNA	5’ → 3’	dNMPs, ssDNA
ExoV	ss/dsDNA	both	short oligos
DNase I	ss/dsDNA	endonuclease	dNMPs, oligos, ssDNA
RNase H[24]	RNA	3’ → 5’	dNMPs
RNase T[20]	ssDNA/RNA	3’ → 5’	dNMPs

The focus of this study is Exonuclease III (from now on ExoIII), an exonuclease that hydrolyzes the phosphodiester bonds on dsDNA in a stepwise fashion from the 3' end of a substrate strand and releases 5'-phosphomononucleotides as a result (**Fig. 2**).[12] ExoIII cleaves only one strand of the dsDNA and is capable of interacting wither both blunt and sticky ends as well as nicks in the circular DNA.[19] The processivity of ExoIII depends on the temperature of the environment, with the decreasing processive character as the temperature rises to physiological conditions.[23] Like many exonucleases mentioned above, ExoIII's activity is also affected by the presence of bivalent coordinating metal ions such as Mg^{2+} or Ca^{2+}.[26] These metal cofactors are known to enhance nucleases’ catalytic activity through transition-state stabilization via hydrogen bonding and other intermolecular interactions.[27,28]

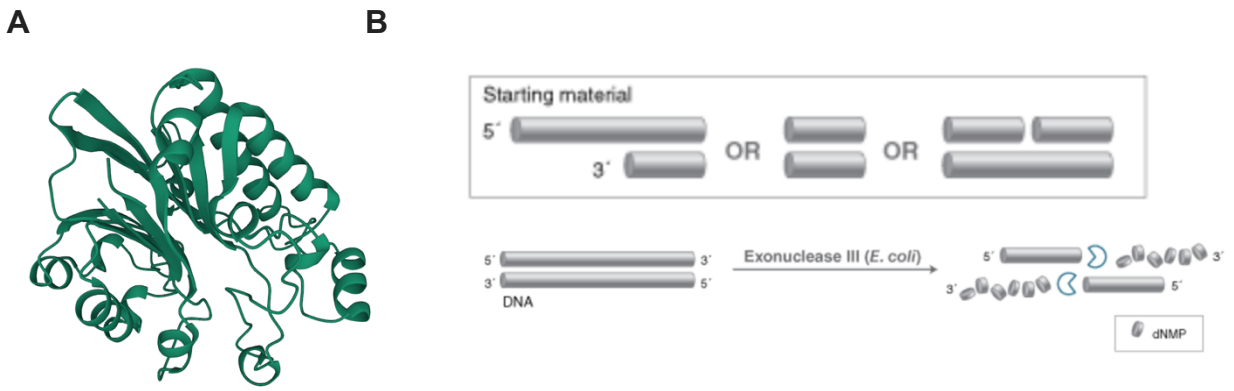

Figure 2. Structure and functionality of Exonuclease III (ExoIII).[13] ***A.*** *A secondary structure of an ExoIII protein generally maintains an alpha-helix formation.*[29] ***B.*** *ExoIII processively cleaves from 3' end of a dsDNA regardless of whether the substrate has blunt or sticky ends, or if any internal nicks are present.*[30]

ExoIII exonuclease activity plays a crucial role in its capabilities of removing 3' nucleotides damaged by radiation or oxidation during the DNA repair process.[31] In addition to hydrolysis of DNA from a 3'-end, ExoIII can act as an endonuclease of apurinic/apyrimidinic (AP) sites[32] and thus promote the incision of abasic sites in the substrate strand.[12] ExoIII also possesses RNase H activity, allowing the degradation of RNA:DNA hybrids present in the solution.[12,13] Overall, a complex of ExoIII activities and properties makes this enzyme an energy-efficient and versatile tool for DNA repair in cells of numerous species, from prokaryotes to mammals.

In recent decades, ExoIII has been extensively used in biological and biochemical research as a convenient enzyme for preparing single-stranded DNA for dideoxy sequencing[33], making nested deletions in double-stranded DNA[34], or site-directed mutagenesis[30,35]. Moreover, ExoIII has been implemented in more advanced

biotechnological designs, such as DNA molecular motors.[36] The study of ExoIII kinetic capabilities will serve as a basis for its utilization in the first RNA-free rolling motor.

Molecular machines or motors are constructs capable of transferring the chemical energy of various sources into a clear mechanical output given a specific stimulus.[37] Biomolecules generating mechanical motion due to an exothermal chemical reaction are abundant and vital for living organisms, presiding over such processes as ATP generation by ATP synthase[38] or a movement of a kinesin protein[39] along the microtubule filaments. Other crucial biological functions of molecular machines include translation[40], DNA replication[41], intracellular transport, and muscle contraction[42].

ATP synthase is an enzyme catalyzing the ATP generation on the inner membrane of eukaryotic mitochondria or prokaryotic plasma membrane. A complex structure consisting of two rotary motors, the proton-driven intrinsic domain F_0 and the ATP-driven globular catalytic domain F_1, ATP synthase synthesizes ATP from ADP and Pi via rotary catalysis of two domains (**Fig. 3**).[38] The energy powering the motor stems from the gradient of the electrochemical potential of protons between the inner and outer sides of the membrane.[38,42] The accumulation of protons on the inner side of the membrane occurs in electron chains of respiration or photosynthesis, specifically through biochemical pathways involving NADH dehydrogenase, cytochrome bc1 complex, or cytochrome c oxidase.[38] With a large electrochemical potential, protons flow through F_0, driving the movement of its rotor.[43] The side stalk connecting two domains of ATP synthase allows the rotor of F_0 to promote the rotation of the ATP-generating F_1 assembly. The reverse

reaction, ATP hydrolysis, is facilitated by the rotation of the motors in the opposite direction and, thus, a build-up of protons on the inner side of the membrane.[43]

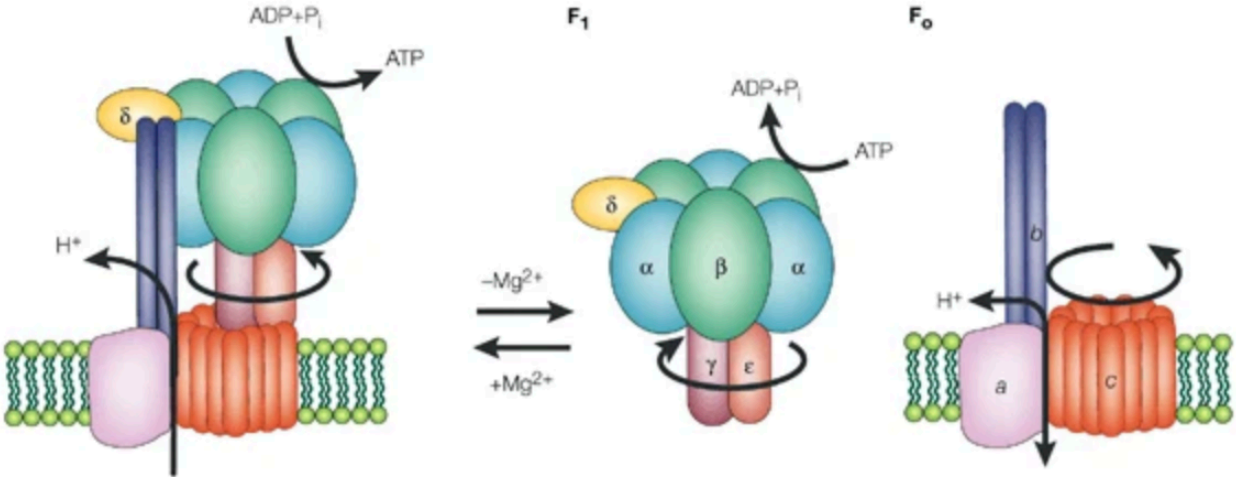

Figure 3. Structure and functionality of the ATP synthase.[43] *Two connected ATP synthases domains rotate due to the electrochemical potential created by the proton gradient and synthesize ATP from ADP and Pi as a result. The reaction is reversable. Reproduced from Reference 43 (CC BY-NC 3.0).*

Another example of molecular motors in the cell is kinesin superfamily proteins, which, together with dyneins and myosins, are responsible for intracellular transport with the energy generated by ATP hydrolysis.[44] While dyneins are involved in the motility of cilia and flagella[45] and myosins' movement along actin filaments is responsible for muscle contraction[46], kinesins transport proteins and mRNAs along cytoskeleton filaments[47], especially in a polarized environment of neurons or epithelial cells. Kinesins consist of a highly conserved motor domain and unique stalk and tail domains depending on the motor's target cargo and scaffolds. Conventional kinesins (Kinesin 1) employ the "hand-

overhand" model of two motor domains stepping processively along microtubules (**Fig. 4**).[39,48]

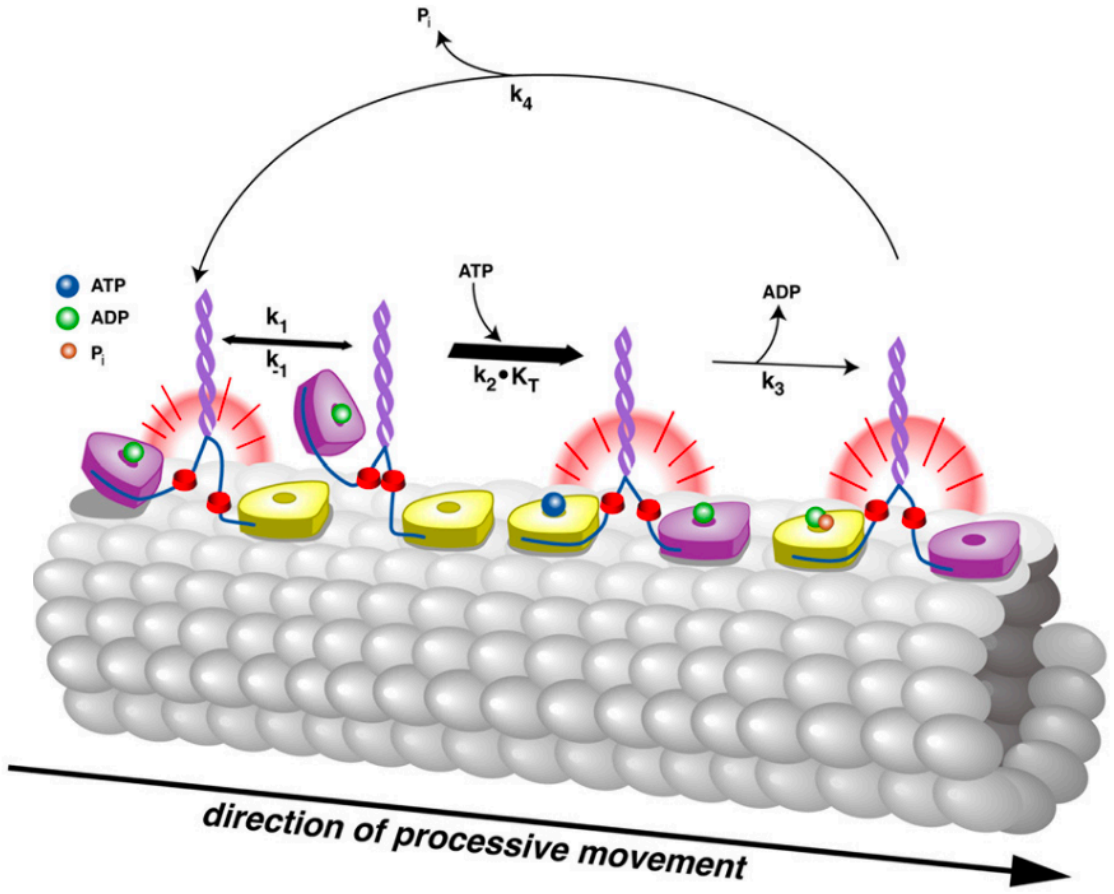

Figure 4. Structure and functionality of the kinesin motor.[48] *Kinesin triangular heads move processively and directionally via the neck linkers along the microtubule track. The walking movement is powered by the ATP hydrolysis, and the four-step mechanochemical cycle is governed by the balance of kinetic rates of unit association, conformational change, and dissociation. Reproduced from Reference 48 (CC BY-NC 3.0).*

Fascinated by the variety and functionality of molecular motors in nature, scientists have long attempted to replicate such systems and design assemblies generating and controlling mechanical motion at the molecular scale.[49] The advances in supramolecular chemistry and nanotechnology allowed scientists to construct complex structures capable of processive displacement, response to external stimuli, and dynamic force generating[49], including synthetic muscles[50], shuttles[51], walkers[52], rollers, pumps[53], elevators, switches[54], hinges[54], balances[55], propellers[56], and nanocars[57]. This emerging variety of molecular motors is controlled by either light, chemical reactions, or electrochemical potential. The expanding repertoire of artificial molecular motors has been used in a variety of biotechnological applications, from smart polymers to catalysis to drug delivery.[49]

One of the first breakthroughs in the field was established by Jean-Pierre Sauvage at the University of Strasbourg with his development of catenane, a structure consisting of two interlocked macrocycles that can freely rotate around each other (**Fig. 5, A**).[58] The next major step in synthesizing artificial motors was rotaxane devised by Fraser Stoddard from Northwestern University.[54,59] Rotaxane is a primary example of a molecular shuttle, a construct in which a macrocyclic wheel engaged in a translational movement along the axle thread between two sites (**Fig. 5, B**).[60] The motion of these first-generation artificial motors was controlled by the electrochemical interactions between their individual parts. Bernard Feringa from the University of Groningen has been credited for his outstanding work with rotary motors that uses photoisomerization of a double bond as a rotary axle to stimulate movement (**Fig. 5, C**).[49,54] For these groundbreaking achievements in the

synthesis and application of early-generation molecular motors, Jean-Pierre Sauvage, Fraser Stoddard, and Bernard Feringa were awarded a Nobel Prize in Chemistry in 2016.[61]

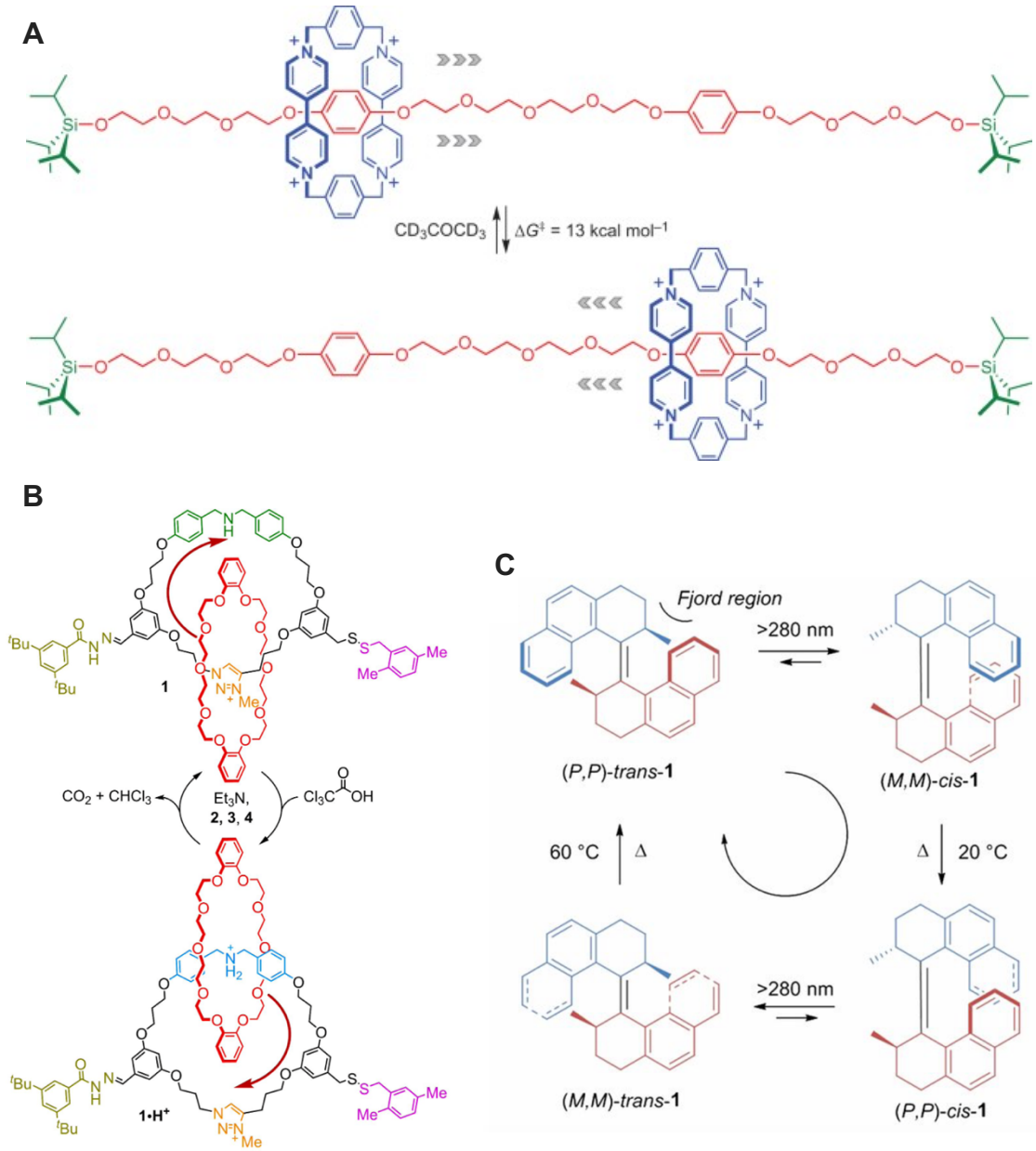

Figure 5. Examples of early-generation artificial molecular motors (AMMs). ***A.*** *A rotaxane developed by F. Stoddard is a molecular shuttle in which a macrocyclic ring traverses between two ends of the axle thread.*[60] ***B.*** *A catenane developed by J.-P. Sauvage has two interlocked rings capable of rotating around the axes triggered by the external chemical stimuli.*[62] ***C.*** *A rotary motor developed by B. Feringa employs the photoisomerization of the double bond to power the rotation of its fragments.*[49] *Reproduced from References 60, 62, 49 (CC BY-NC 3.0).*

Taking inspiration from a bipedal "walking" movement of kinesins and myosins across microtubules and actin filaments, researchers have constructed a number of linear molecular motors in which a two-legged unit is capable of walking up and down a molecular track. A challenge in designing such a system is that per each step, one leg of a motor must be labile to drive the movement while the other has to be attached to generate a temporary pivotal point.[62] In *Delius et al.*, a small-molecule motor propagates on the four-foothold molecular track in response to the pH change of the environment. (**Fig. 6**).[62] In acidic conditions, one of the feet is locked by the disulfide bond, while the hydrazone unit is labile and capable of interacting with track footholds before or after it.[63] Conversely, in basic conditions, the hydrazone unit is attached to the foothold, and the disulfide unit seeks a binding site.[63] The switch in the acidity of the environment allows a walker to randomly and processively move along the track. The design mimics the principle of mechanical translocation of natural linear motors and serves as a blueprint for future small-molecule walkers performing complex tasks in biological settings.

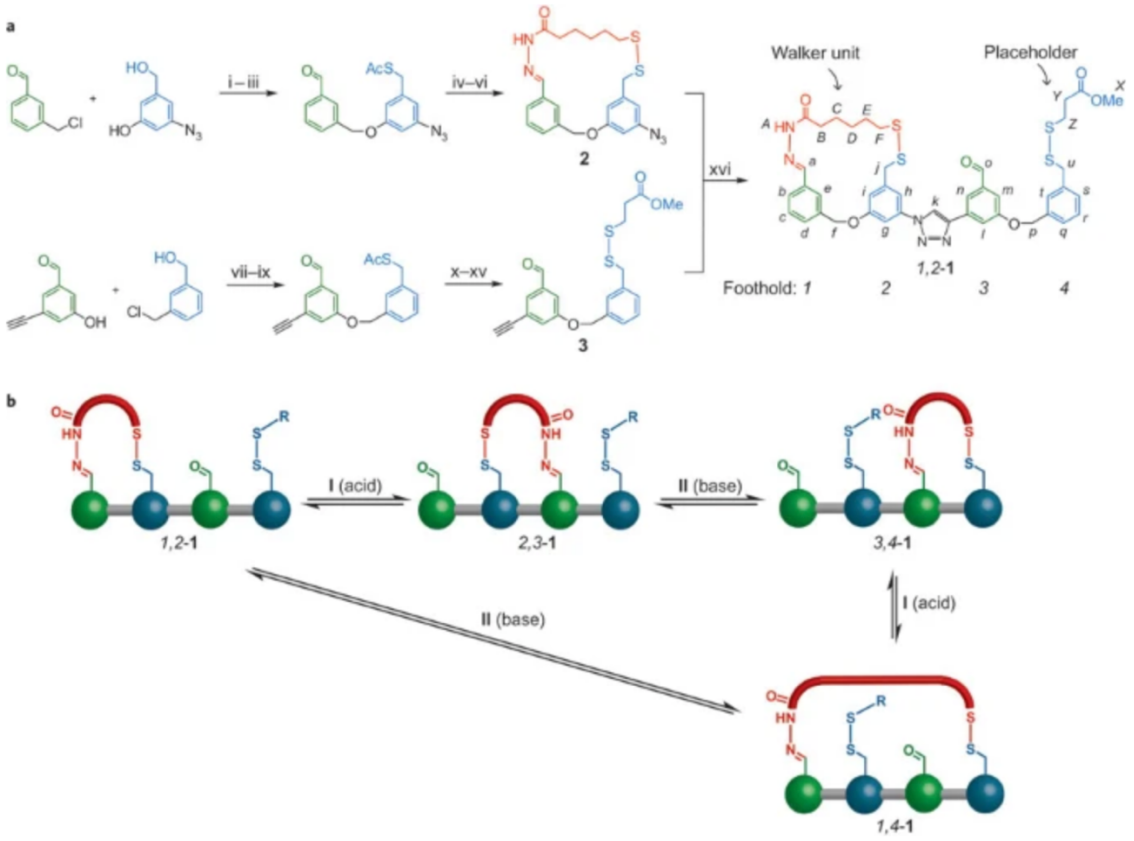

Figure 6. Translocation of a small molecule-based synthetic bipedal walker.[62] *A small molecule moves along the sites of the track via either disulfide or hydrazone bond. The walking is controlled by the pH changes of the external environment. Reproduced from Reference 62 with a permission from Nature Chemistry.*

Mimicking natural machinery performing complex tasks requires sophisticated architecture as well as a high level of controllability and flexibility of artificial motors.[59] Unfortunately for its implementation as synthetic machines, designs consisting of small molecules and organic compounds often lack these properties.[64] Attempting to resemble the dimensions and structural intricacy of biological motors, scientists have devised a new generation of motors utilizing DNA nucleotides as building blocks of larger designs. DNA

has become an attractive biopolymer for constructing artificial motors for multiple reasons. First, its broad availability and high customizability make testing, optimizing, and tuning motors' structures an easier and faster task.[65] DNA's chemical stability greatly exceeds that of proteins or RNA, adding to the motor's overall durability. Other qualities of DNA that have been useful in developing DNA nanostructures, known as DNA origami, are its localized stiffness[59] (ability to vary flexible and rigid elements) and effective persistence length[59] (high level of bending before folding). The sum of these parameters opened new possibilities for assembling DNA-based motors with even greater functionality and scope of applications.

The work done by Jong-Shik Shin and Niles A. Pierce has shown a new direction in DNA nanoengineering: the development of DNA-based walkers.[66] Taking inspiration from the principle of movement of kinesin along the microtubule, these scientists have constructed a DNA walker strand with two "legs" processively bridging with the sites along the DNA track via attachment strands and unbinding from the track upon the addition of disattachment strands (**Fig. 7**).[66] The so-called strand displacement reaction allows a processive propagation of the walker along the track of six binding sites. Walking is controlled by the addition of attachment and disattachment strands, meaning that the designed DNA motor produces directed movement only with the external stimulus.[66]

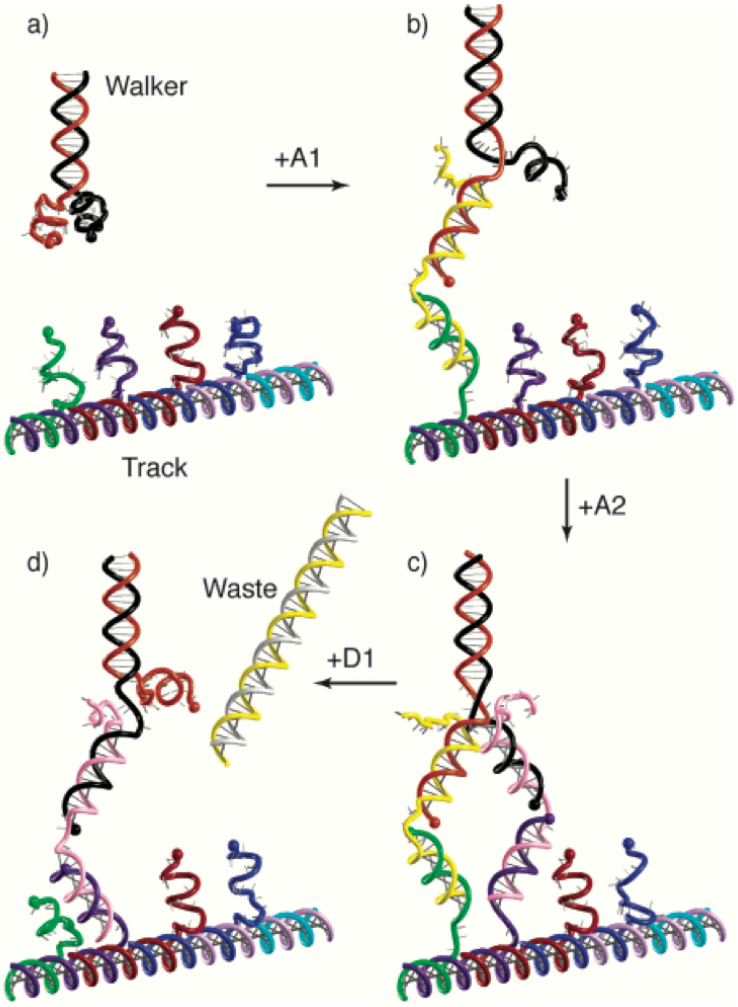

Figure 7. Translocation of a DNA-based synthetic bipedal walker.[66] *A bipedal DNA walker consists of a walker, a track, attachment and detachment strands. The movement is powered by (1) binding of two attachment strands to the track, (2) binding of the detachment strand that causes a strand displacement of the neighboring leg. Reproduced from Reference 66 with a permission from American Chemical Society.*

Another significant step forward in designing DNA-based molecular machines is the invention of the DNA lame walker, a strand with two legs randomly and autonomously moving along the surface of a microsphere (**Fig. 8**).[67] A stochastic DNA walker, in this

case, consists of a long leg responsible for the movement and association, while a short leg rapidly searches for the following binding site on the particle.[67] In contrast to the walking system described before, this walker is powered by the nicking endonuclease cleavage rather than a strand displacement mechanism. The construct's processivity and performance lead to its effective application in detecting target DNA with a high level of specificity.[67]

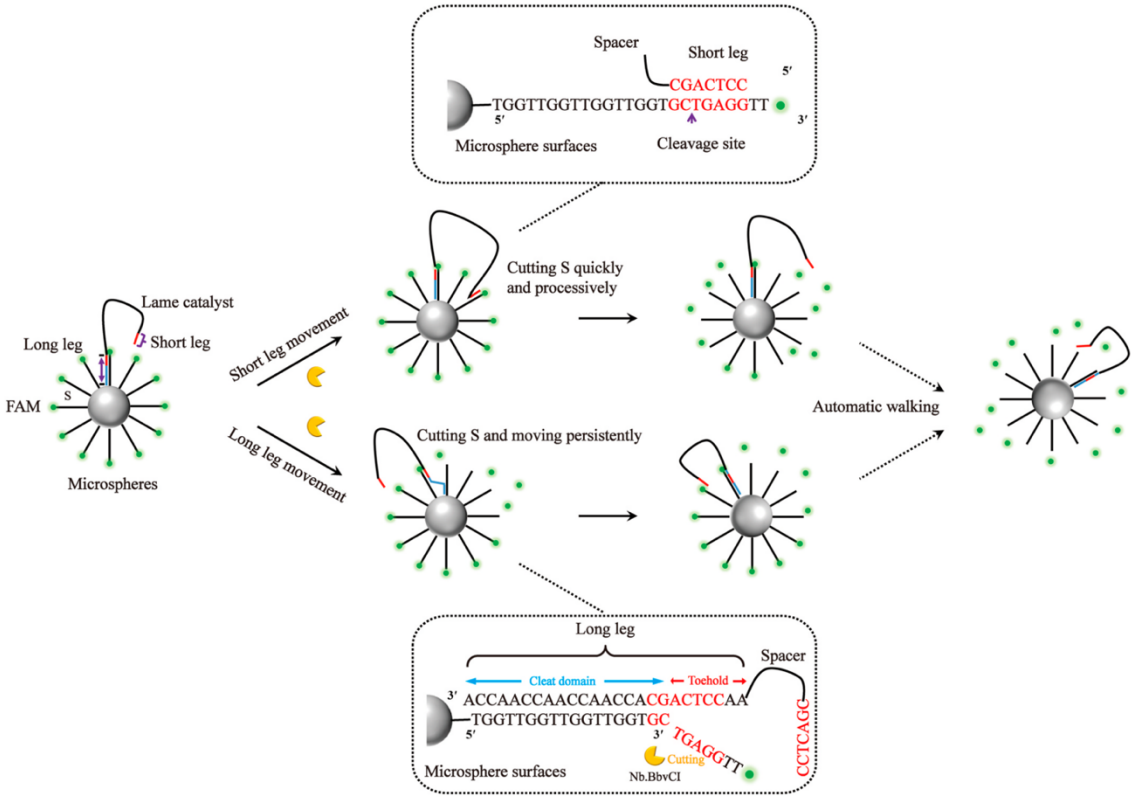

Figure 8. Translocation of a synthetic DNA walker on a microsphere powered by the cleavage of the nicking enzyme.[67] *A lame DNA walker persistently moves on the surface of the microsphere, binding a long and a short leg to the anchor strands. The movement is powered by the enzymatic cleavage of the binding region by the nicking*

enzyme Nb.BbvCI. Reproduced from Reference 67 with a permission from Biosensors and Bioelectronics.

DNA-based walkers described above, as well as numerous other versions with altered designs and applications, are considered to be breakthroughs in the field of DNA biophysics and nanoengineering. Yet the implementation and advancement of this technology have been hindered by several potent scientific challenges and trade-offs. First, the maximum distance the best DNA walkers can propagate is 1 um, highlighting the difficulty of preserving the track affinity and motor endurance in the system.[65,68] Increasing the multivalency of the walker solves some of the issues regarding fidelity yet significantly slows down the motor.[68] Currently, the limit for the rate of DNA walkers is set as 1 nm/min.[68] Indeed, it turns out that the mean distance traveled and the mean velocity of the motor traveling that distance are two target goals colliding with each other and leading scientists towards an uncomfortable decision of what parameter to prioritize in their design.[69]

Kevin Yehl and colleagues at the Salaita group described a system in *Yehl et al.* that untangles the mentioned trade-off and increases both the distance traveled and velocity of the motor by orders of magnitude.[68] An elegant solution to the problem, in this case, was to introduce a completely different mode of motion: rolling. The proposed system consists of a DNA-coated particle hybridized to the complementary RNA monolayer on a gold surface (**Fig. 9**). Upon the addition of RNase H, which selectivity hydrolyzes dsRNA that links the motor to the surface, the substrate gets consumed, and the motion of the rolling motor is directed away from the areas of the cleaved substrate.[68] This phenomenon

is described as a "burnt-bridge Brownian ratchet," previously employed in DNA walkers and spiders. What is novel about Yehl's system is the proposed utilization of a spherical bead which significantly increases the contact area and, thus, multivalency of the motor compared to previously reported constructs.[70] It is important to note that even with an increased multiplicity, the speed of the motor is not impaired due to a high level of processivity and turnover of RNase H compared to enzymes commonly employed in DNA walkers. The unique "cog-on-wheel" design allows the rolling motors to travel in a super-diffusive, self-avoiding manner for, on average, 380 ± 50 nm with a speed of about 2 μm/min (**Fig. 9**).[68] A particle displacement readout of the proposed motor system was able to detect single nucleotide polymorphism using a smartphone camera.[68] This newly invented mechanism defies previously established limitations and brings new possibilities to creating next-generation molecular machines employed in future biosensing, drug delivery, and computational efforts.

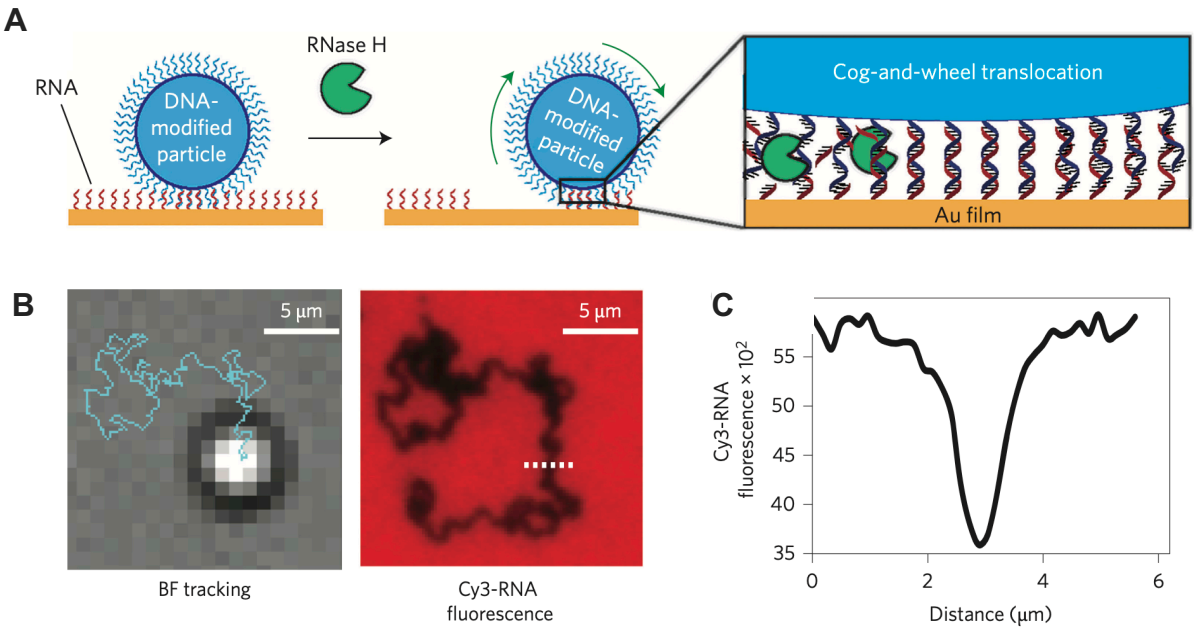

Figure 9. Translocation of a synthetic DNA-based rolling motor on RNA monolayer fabricated on a thin gold film.[70] ***A.*** *A schematic shows the principle of the rolling motion of the DNA-modified particle on an RNA layer via cog-and-wheel translocation.* ***B.*** *Representative BF and TRITC (Cy3-fluorescence) image depicting a single particle's locomotion track over 30 mins after RNase H addition.* ***C.*** *The line-scan plot from B showing a Cy3 signal depletion in the track region. Reproduced from Reference 70 with a permission from Nature Nanotechnology.*

Over the years, the Salaita lab group have expanded on this invention and attempted to modify the design to achieve even higher processivity and endurance. In *Bazrafshan et al.*, Alisina Bazrasfshan and colleagues have used DNA origami structure instead of a particle as a nanomotor. A bundle of 16 DNA double helices formed into a rectangular prism with outstanding DNA legs was reported to show a ballistic, unidirectional, linear movement over micron distances at an average velocity of 40 nm/min (**Fig. 10**).[65] Another

advantageous characteristic of a DNA origami nanomotor is its high tunability of numerous system parameters, such as leg distribution and body rigidity.[65] In addition to the assembly of more optimal DNA rolling motors, the study has explained some of the previously obscure structure-function dependencies regarding the role of shape, leg density, and chassis flexibility in enhancing the performance of motors.[65]

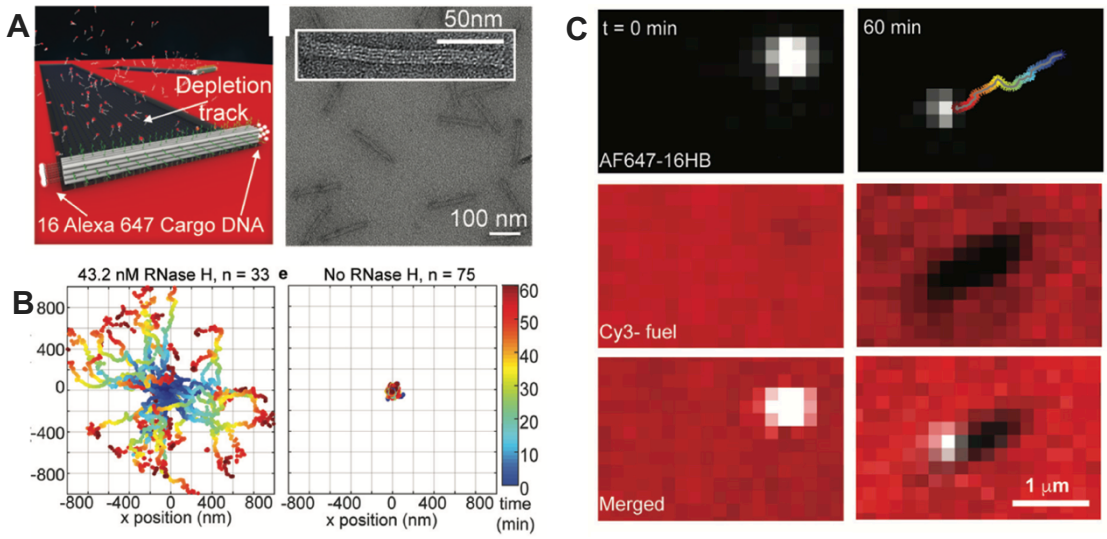

Figure 10. Tunable DNA origami motor travelling ballistically over micron-scale distances.[65] ***A.*** *A schematic and a TEM image of 16 HB origami motor.* ***B.*** *A ensemble plot showing the trajectories of motors (n = 33) with 43.2 nM RNase H (left) and no enzyme added (right).* ***C.*** *Time-lapse fluorescence images of A647-16HB, Cy3-fuel, and overlay of a single origami motor. The color bar after 60 min time-lapse demonstrates a ballistic motion of the motor. Reproduced from Reference 65 with a permission from Angewandte Chemie International Edition.*

Tackling the challenges and opportunities that DNA rolling motors bring, our group has focused efforts on (1) developing the fundamental knowledge of the thermodynamic and kinetic phenomena at the interface of the enzyme-substrate interaction, (2) tuning and optimizing motors' performance by changing various systemic parameters, and (3) exploring the potential *in vitro* and *in vivo* applications of the construct.[65,69–72] The first task aims to address incremental yet necessary questions about the interplay between kinetic constants (k_{on}, k_{cat}, k_{off}) governing the movement of the motor as well as the role of the DNA/RNA length, stability, and rigidity in creating an optimal molecular machine. For the second task, lab members attempted to switch the type of enzyme and surface, introduce microfluidic flow and enzyme-free platforms, and alter the buffer composition, beads' size and shape, DNA/RNA sequence and GC content – all in the process of evolving the initial design into a more robust and controllable shape. Indeed, the achieved versatility brings greater familiarity and understanding of the underlying mechanism of the system.

The third, application-oriented task pushed our group to think of the advantages our model has over the existing scope of bioanalytical methods. The remarkable selectivity and specificity of DNA nanomotors in detecting nucleic acids and viral particles, including the ones of SARS-CoV-2, hold immense potential for our system in piloting and, subsequently, manufacturing novel biosensing tools. Another strength is the possibility of cross-communication between multiple types of particles, which was explored in *Piranej et al.* and resulted in the creation of the simplest logic gates. This important milestone marks motors' future promise as a blueprint for biocomputational technologies. And,

finally, a far-ahead goal of the group is to develop DNA rolling motors capable of translocating *in vivo*, turning targeted drug-delivery nanomachines rolling on the organelle, cell, and tissue surfaces into a reality.

A project my graduate mentor, Yusha Imtiaz, and I have been working on entails using ExoIII to power the RNA-free, DNA-only nanomotors rolling on a DNA-modified glass surface. The schematic design and early data showing moderate motor translocation is shown in **Fig. 11**. The principle of motion via the burnt-bridge Brownian ratchet in this project is reminiscent of the one previously reported in *Yehl et al.* and *Bazrafshan et al.*, yet the design of ExoIII-powered motors avoids the dependence on the RNA monolayer or RNA/DNA chimera hybrids.[65,70] The reasoning behind such avoidance is RNA's instability and inapplicability in environments rich with RNases. Additionally, utilizing just one type of nucleic acid in the motor system simplifies experiments' general architecture and workflow. Exonuclease III (ExoIII) was picked over other candidates, which included exonucleases, nicking enzymes, and Cas12, due to its processive cleavage of dsDNA, commercial availability, and a precedent of use in DNA-based walker designs.

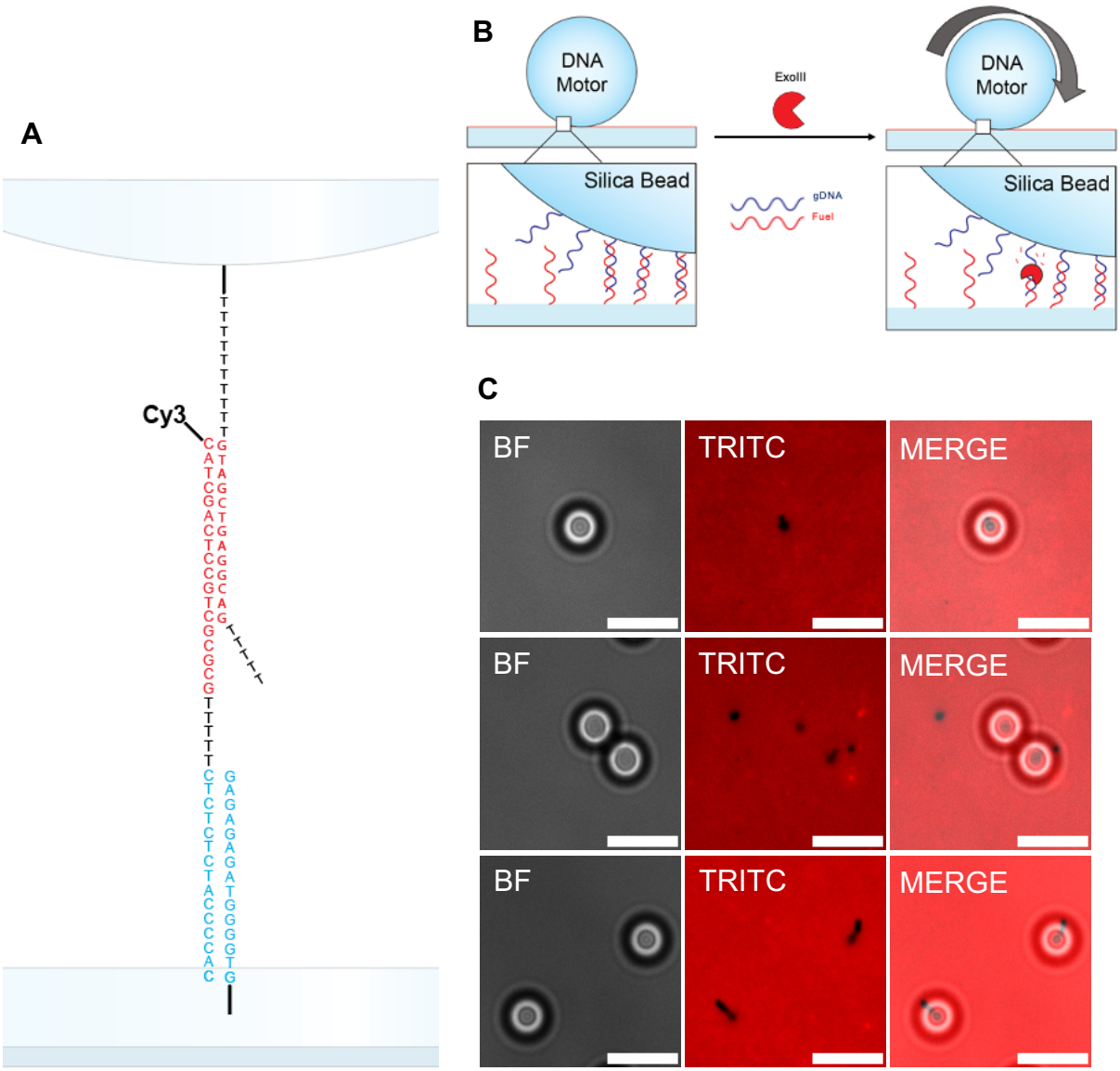

Figure 11. A proposed RNA-free, next-generation rolling motor (unpublished by Y. Imtiaz). ***A.*** *A proposed sequence for the fuel and gDNA strands used in the preliminary studies.* ***B.*** *A schematic depicting the principle of motion of the DNA motor reminiscent of the previously reported RNA-dependent, RNase H-powered rolling motors.* ***C.*** *An initial data depicting small track formation on the BF, TRITC (Cy3-fluorescence), and merged microscope images.*

In order to obtain the processive rolling of the nanomotor on the surface, three rates must be closely monitored: the rate of hybridization of the DNA leg to the surface monolayer (k_{on}), the rate of enzymatic cleavage of the surface-bound double-stranded substrate (k_{cat}), and the rate of unzipping of the DNA leg from the consumed substrate (k_{off}). The balance between these three kinetic constants ensures a super-diffusive motion of the particle, while the failure to maintain it leads to either particle stalling or floating. Previous studies have done much work to uncover the kinetics of RNase H powering the DNA/RNA motors' movement. However, little is known about the kinetic capabilities of ExoIII with short oligonucleotides under the conditions set for the translocation of the DNA motor. Previous literature on enzyme kinetics of ExoIII is largely outdated and does not give reliable estimates of its cleavage rates of short DNA fragments in both in-solution and on-surface environments.

In its essence, this study is aimed to address the gap in knowledge of ExoIII's behavior with DNA substrates under different conditions – freely floating and immobilized. Besides, the enzyme's cleavage viability against common protecting groups is assessed. The findings of the study contribute to the larger project of designing RNA-free rolling motors with ExoIII. Series of experiments are conducted to discover the optimal system parameters for both kinetic assays and rolling experiments. In the longer term, elucidation of ExoIII's potential in highly multivalent, processive rolling motors opens new possibilities in the field of DNA nanotechnology, promoting progress towards better and faster molecular motors performing tightly controlled, sophisticated tasks reminiscent of the natural biological machinery.

Methods

Sections '*Glass surface preparation and etching'* and '*Fabrication of the DNA monolayer on a glass surface*' were adapted from the protocol design of Alisina Bazrafshan described in *Bazrasfhan et al.* with minor variations and additions.[65] Sections *'Thermal evaporation of gold films', 'Fabrication of the DNA monolayer on a gold surface'*, and *'Microscopy'* were adapted from the protocol design of Selma Piranej described in *Piranej et al.* and accompanied supplementary information.[71]

Materials

All chemicals were purchased from Sigma-Aldrich unless otherwise noted. All DNA oligonucleotides were obtained from Integrated DNA Technologies (Coralville, IA), stored at –20 ºC, and used without purification. The sequences of all oligonucleotides used in the experiments, including fluorescently labeled and modified, are shown in the Table X. In case of unavailability of the desired modifications, Cy3-NHS, Cy3B-NHS, FAM-NHS, and Cy5-NHS fluorescent dyes and alkyne-modified oligonucleotides were purchased separately from Integrated DNA Technologies (Coralville, IA). Fluorophores and oligonucleotides were conjugated and later isolated by the HPLC. Stock solutions and aliquots were prepared using Nanopure water (Barnstead™ Nanopure™ system, resistivity = 18.2 MΩ, Thermofisher, Waltham, MA), from now on referred as DI water. ExoIII was obtained from New England Biolabs (Ipswich, MA).

Table 2. All DNA oligonucleotides used in the study.

ID	Sequences (5'-3')
Cy3-Fuel (in-solution)	/Cy3/CTG CCT CAG CTA C
Cy3-Fuel (on-surface)	CACCCCATCTCTCTCT$_5$ CTGCCTCAGCTAC/Cy3/
FAM-Fuel	CACCCCATCTCTCTCT$_5$ CTGCCTCAGCTAC/FAM/
gDNA	GTA GCT GAG GCA G
BHQ2-gDNA	GTA GCT GAG GCA G/BHQ2/
gDNA-T5	GTA GCT GAG GCA GTT TTT
Inverted gDNA	GTA GCT GAG GCA GT*T* T*T*/3InvdT/
Cy5-gDNA	GTA GCT GAG GCA G/Cy5/
DNA anchor (glass)	GAGAGAGATGGGGTGT$_{15}$/5-Hexynyl/
DNA anchor (gold)	/5AmMC6/GAGAGAGATGGGGTGT$_{15}$/3ThiolMC3-D/

In-solution kinetic assay

Oligonucleotides purchased from Integrated DNA Technologies were annealed at 95 ºC in a Bio-Rad T100 thermal cycler from Bio-Rad Laboratories (Hercules, CA) and then gradually cooled down to 25 ºC for about 90 mins. The obtained products were pipetted into the 96-well plates along with the buffer (150 mM NaCl, 60 mM Tris-HCl, 5-15 mM $MgCl_2$) and 1 mM DTT. ExoIII was added right before the kinetic readout, ensuring the immediate measurement of the initial cleavage of substrate. The fluorescence intensity (540/590 nm excitation/emission for Cy3/Cy3B signals, 485/528 nm excitation/emission for FAM signal) of each well were detected with a Bio-Tek Synergy HT plate reader to

measure a real-time fluorescence intensity change due to the increase of the distance between the quencher and the quenched fluorophore as a result of a cleavage.

PAGE Gel electrophoresis

To cast a 20% denaturing polyacrylamide (PAGE) gel, a mixture consisting of 10 mL 40% 29:1 acrylamide/bis, 7.2 g urea, 2 mL 10X TBE buffer, and 2.55 mL DI H_2O was made in a 50 mL falcon tube and thoroughly shaken until a nearly complete dissolvement of urea. Then, 12 µL TEMED and 60 µL 30% (w/v) ammonium persulfate (APS) were added to begin the activation of the polymerization. The solution was quickly vortexed and poured in between a set of 0.75 mm gel plates (Bio-Rad, Hercules, CA). After approximately 30 mins, polymerization was complete, and the obtained PAGE gel was fully solidified. The gel plates were wrapped in a wet tissue and stored at –4 ºC for 1-3 days after the casting.

In preparation of samples for the gel electrophoresis, a uniform final concentration of DNA oligonucleotide probes (100 nM) was used. Depending on the condition tested, various concentrations of ExoIII (0 nM, 8 nM, 40 nM) were added. Annealing of the DNA substrate strands was done in a Bio-Rad T100 thermal cycler from Bio-Rad Laboratories (Hercules, CA) for approximately 90 mins with a stepwise cooling to ensure the stability of the annealed product. The product was then incubated at 37 °C with ExoIII (0 nM, 8 nM, 40 nM) in a Bio-Rad T100 thermal cycler for 20 mins. ExoIII left in the solution was terminated by increasing the temperature of incubation up to 95 °C. 15 µL of the reacted solution was taken and mixed with 3 µL of 1X Purple SDS-free DNA loading dye (NEB, Ipswich, MA). The DNA loading dye used in the electrophoresis consists of 0.042% (w/v) bromophenol blue and 10% (v/v) glycerol.

Electrophoresis was conducted on a Bio-Rad Mini-PROTEAN Tetra Vertical Electrophoresis Cell (Bio-Rad Laboratories, Hercules, CA) and PowerPac™ Basic Power Supply. An empty gel was pre-run before the addition of DNA oligonucleotides at 120V for approximately 15 mins. The gel wells with the DNA probes were held at 170V for approximately 45-60 mins. The completed gel was first imaged on a Cytiva Amersham Typhoon laser-scanning platform using *'Fluorescence mode'* and Cy3, Cy5, or FAM filters to detect the presence of certain dyes on the investigated strands. Finally, the gel was kept in a 50mL 1:10,000 dilution of Promega Diamond™ Nucleic Acid Dye for 10 mins and imaged with the *'Nucleic acid mode'* to make inferences about the presence of specific DNA denatured strands upon the addition of enzyme to the system.

Glass surface preparation and etching[65]

An IBIDI glass slide (No.1.5H, 25 x 75 mm^2) was sonicated in DI water twice for 5 min. The slide was subsequently sonicated in 200 proof ethanol for 15 min. The slide was then thoroughly washed with DI water to eliminate any remains of ethanol on the surface. A piranha solution (v/v = 3:7 hydrogen peroxide/sulfuric acid) was used to etch the glass slide for 30 min leading to the activation of hydroxyl groups and ensuring no contamination with any organic material on the glass. Extreme caution was taken while working with corrosive and potentially explosive (if in contact with organics) piranha solution. Immediately following etching, a slide was placed into a solution containing 2% (v/v) APTES in ethanol for 1 h. Lastly, a slide was washed with ethanol three times and

cured in an oven in 110 ºC for 10 min. The produced slides were used within 1-2 days after the process.

Fabrication of the DNA monolayer on a glass surface[65]

The slides were attached to either six-channel microfluidic cells (Sticky-Slide VI 0.4, IBIDI) or 96-well plates (Corning, ME). To each channel or well, approximately 50 µL of 10 mg/mL of NHS-PEG_4-azide (Click Chemistry Tools) in 0.1 M $NaHCO_3$ (pH = 9) were added, and the solution was incubated for 1 h. Upon incubation, the channels or wells were washed with DI water under a constant flow powered by the vacuum suction. After a thorough rinse, a solution of 10 µM alkyne modified DNA anchor strand, 50 µM THTPA, 10 µM $CuSO_4$ and 1 mM sodium ascorbate in 1 M potassium phosphate buffer was added to the surface and incubated for 1 h. Excess DNA was then removed from the channel or well with a constant flow of approximately 5 mL of DI water. A complimentary was DNA strand (100 nM) was then added to the channels or wells; the plate was parafilmed and left overnight at room temperature. The DNA monolayer remained intact within one-two days after the process (**Fig. 12**).

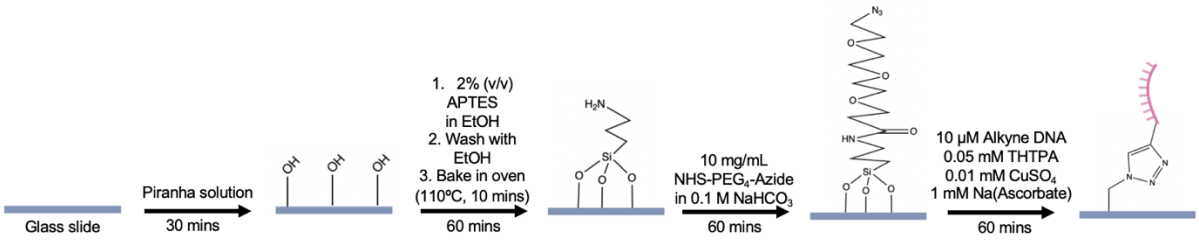

Figure 12. Glass slides preparation. A scheme summarizing the procedure for preparing and functionalizing the glass slides.

Thermal evaporation of gold films[71]

An IBIDI glass slide (No.1.5H, 25 x 75 mm^2) was sonicated in DI water twice for 5 minutes. The slide was subsequently sonicated in 200 proof ethanol (Fisher Scientific, 04-355-223) for 5 minutes and dried under a constant flow of N_2. A slide was transferred into a thermal evaporator chamber with a constant pressure of 50 x 10^{-3} torr. After three purges with N_2, the pressure was decreased to 2 x 10^{-3} torr. Under this pressure, a 3-nm Cr film was added onto the glass slide at a rate of 0.2 Å s^{-1}. Following the adhesion of Cr layer, 6-nm Au layer was added at a rate of 0.4 Å s^{-1}. The produced slides were used within 1 week after the process (**Fig. 13**).

Fabrication of the DNA monolayer on a gold surface[71]

The slides were attached to six-channel microfluidic cells (Sticky-Slide VI 0.4, IBIDI). Prior to functionalization of the surface, each channel was washed with 5 mL of DI water. Approximately 50 µL of thiol-modified DNA anchor in 1M potassium hydrophosphate buffer were added to each channel, and the solution was incubated overnight. The gold film was parafilmed to prevent evaporation. Upon incubation, excess DNA was removed by rinsing each channel with 5 mL of DI water. A complimentary was DNA strand (100 nM) was then added to the channels; the plate was parafilmed and left overnight at room temperature. The DNA monolayer remained intact within one-two days after the hybridization (**Fig. 13**).

Figure 13. Gold slides preparation. A scheme summarizing the procedure for preparing and functionalizing the gold slides.

Microscopy[71]

Optical microscope imaging was done on Eclipse Ti2-E Nikon Inverted Research Microscope with the Elements software package (Nikon). An automated scanning stage, a 1.49 NA CFI Apo TIRF x100 objective, a Prime 95B 25 mm scientific complementary metal oxide semiconductor camera, and a SOLA SE II 365 Light Engine as a white-light excitation source were used to capture images and record the time-lapses. Fluorescence signals of Cy3, Cy5, and FAM were collected with a TRITC filter set (Chroma, 96321), an EGFP/FITC/Cy2/Alexa Fluor 488 filter set (Chroma, 96226) and a Cy5/Alexa Fluor 647/Draq 5 filter set (Chroma, 96232) with an exposure time of 100 ms.

Data analysis and acquisition

Microscope image processing was conducted in Fiji (ImageJ). A Fiji extension allowed a direct transfer from Nikon Elements file (.nd2) into the ImageJ system for subsequent surface fluorescence intensity analysis. Gel electrophoresis analysis stayed mostly qualitative. The rest of the statistical inferences, calculations, and graphs were performed in GraphPad (v.9.1.0).

Results and Discussion

Enzyme kinetics of exonucleases is dependent on multiple factors, including but not limited to substrate and enzyme concentrations, intrinsic properties of the enzyme, DNA sequence and GC content of a substrate, the steric availability of the substrate cleavage sites, presence of coordinating ions, and other buffer conditions.[12] Throughout this study, we scanned multiple experimental conditions, changing one parameter at a time. This stepwise approach allowed us to determine the optimal conditions for a moderate and processive cleavage of freely floating short oligonucleotides by Exonuclease III and establish the kcat of the enzyme in solution.

However, the rolling motor design devised by our group employs the enzymatic cleavage of the substrate in a drastically different condition – attached to the surface. The steric rigidity of the substrate immobilized on the surface changes the kinetics of the interaction of enzyme and substrate, demanding another measurement of the enzymatic k_{cat}. Microscope imaging of the enzymatic cleavage of DNA substrate functionalized on the glass surface resulted in gaining the k_{cat} of the enzyme with a surface-bound substate. Obtaining the cleavage rates of short oligonucleotides by Exonuclease III in two environments, in solution and on surface, allowed us to establish a quantitative relation between those rates.

Along with the investigation of the kinetic rates of the enzyme, fundamental studies of the ExoIII's interaction with substrate were conducted with denaturing PAGE gel electrophoresis to determine the viability of certain protecting groups.

In-solution kinetic assay setup

In-solution kinetic measurements on the fluorescence plate reader allowed a high throughput, real-time tracking of enzymatic activity on the substrate of varying concentrations and conditions. A general experimental design of this assay is shown in **Fig. 14**. As ExoIII starts hydrolyzing from the 3' end of the dsDNA, the BHQ2 quencher gets cleaved. The increased distance between the Cy3 fluorophore and BHQ2 quencher results in the rise of the Cy3 signal detected by the apparatus. At least three replicates of each kinetic run were conducted, and fluorescence intensity was later calibrated to the concentration of the substrate.

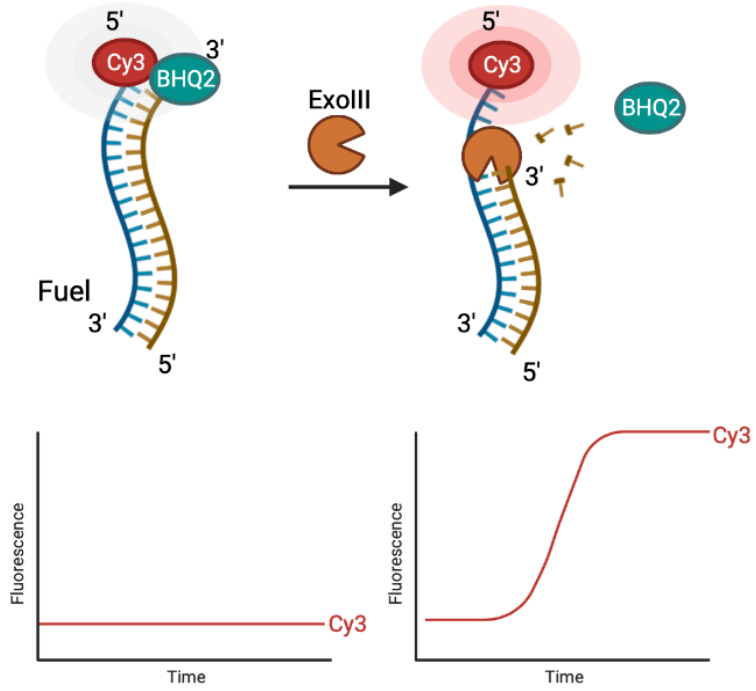

Figure 14. A scheme of the in-solution kinetic assay. *An assay with a Cy3-modified fuel strand and BHQ2-modified gDNA was used to obtain the in-solution k_{cat} of ExoIII based on the change of the Cy3 fluorescence intensity.*

Optimization of enzyme concentration

The first set of experiments aimed to establish the optimal conditions for measuring the in-solution k_{cat} of ExoIII. Different enzyme concentrations of 0.8 nM (0.1 U), 8 nM (1U), and 80 nM (10U) were scanned and plotted against each other to determine an enzyme concentration that provides measurable activity for future experiments (**Fig. 15**). Per our expectations, an increased concentration of ExoIII resulted in increased enzymatic activity and faster substrate cleavage. 0.8 nM (0.1U) of ExoIII proved to be too small for robust substrate cleavage, while 80 nM (10U) of ExoIII promoted too quick of a reaction, with an initial reaction rate undetectable by the plate reader. 8 nM (1U) of ExoIII was established as the optimal concentration of ExoIII and was used in subsequent kinetic assays.

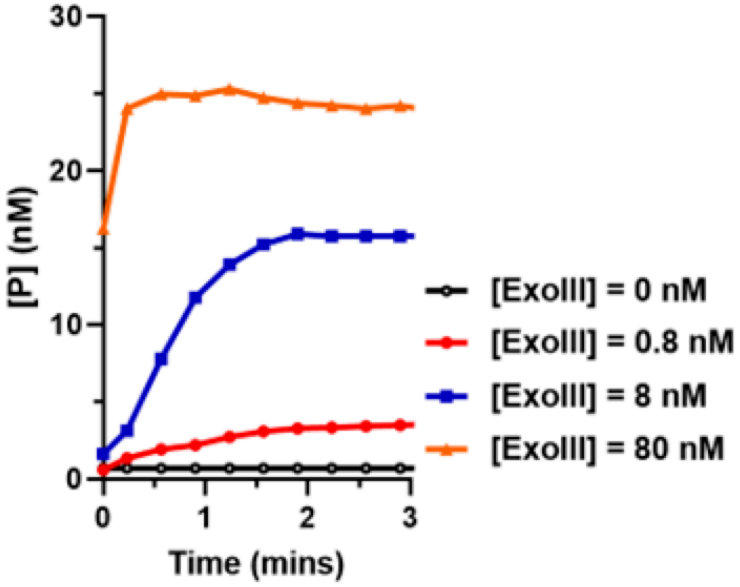

Figure 15. Enzyme concentration dependency. *Too high of the concentration (80 nM) of the enzyme gave an undetected range of measurement of the initial cleavage. Too*

small of the concentration (0.8 nM) of the enzyme did not promote processive cleavage. 8 nm of ExoIII seemed to the most optimal conditions for the subsequent experiments.

Optimization of Mg^{2+} concentration and other buffer conditions

Another factor directly affecting the enzymatic activity of most of the nucleases, including ExoIII, is the presence of Mg^{2+} ions in the system. These abundant divalent ions are considered to be cofactors of ExoIII, which coordinate the enzyme around the substrate and participate in the so-called two-ion catalysis.[26] In addition to enhancing the stability of the enzyme, two Mg^{2+} ions participate in nucleophile formation and product release. The consensus in the literature is that the presence of Mg^{2+} improves substrate recognition and catalytic specificity.[12,19,28] Consequently, we tested the enzymatic activity of 8 nM (1U) of ExoIII with 30 nM of the substrate under different Mg^{2+} conditions (5 mM, 10 mM, and 15 mM) (**Fig. 16**). An increased cleavage rate was observed with a higher concentration of Mg^{2+} ions in the solution.

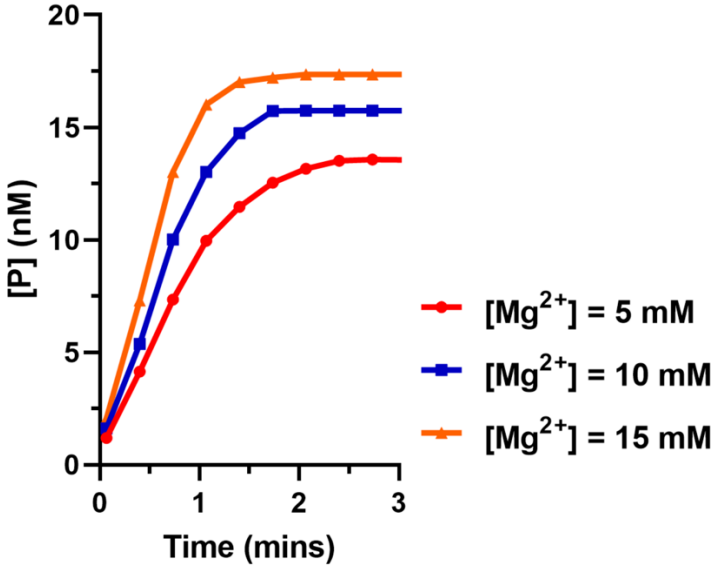

Figure 16. Mg^{2+} concentration dependency. *The concentration of Mg^{2+}cofactor ion affected the activity of the ExoIII. [Mg^{2+}] = 10 mM condition was picked as the optimal setup for future experiments.*

The experiments conducted in this study were performed in the presence of dithiothreitol (DTT) (1 mM), a potent reducing agent that is broadly used in biological assays to stabilize proteins, including nucleases.[73] Additionally, DTT preserves enzymes from irradiative damage in the form of oxygen and nitrogen radicals and prevents the formation of the disulfide bonds in the enzyme.[73] The absence of DTT slowed the enzymatic cleavage of the substrate by ExoIII (not shown). Another factor held constant in this study was the temperature of the solution. Literature suggests that the temperature change from 25 ºC to 36 ºC results in the loss of processivity of ExoIII. With 36 ºC or above, the enzyme behaves distributively, binding and unbinding from the substrate, thus, failing to cleave DNA strands at the same rate as when being processive.[23] To prevent such an event, a constant temperature of 25 ºC was maintained throughout the study. Finally, after test trials in buffers with varying salt concentrations, an optimal buffer was found with 150 mM NaCl, 60 mM Tris-HCl, and 10 mM $MgCl_2$.

These preliminary experiments demonstrated desirable conditions in which the rest of the kinetic assays were conducted. A buffer with specific sodium and magnesium ion concentrations, a constant temperature of 25 ºC, 1 mM of DTT as a reducing agent, and 8 nM (1 U) of ExoIII were kept the same throughout the investigation of the in-solution kinetics of the enzyme to ensure the absence of any confounding variables in the trials.

Obtaining in-solution k_{cat} rate

The ultimate purpose of the in-solution kinetic assay was to determine the kcat of the ExoIII under the specific conditions described above. The concentration-independent kcat can be derived from the maximum velocity of the reaction (V_{max}). A common method to find the V_{max} of an enzymatic reaction, as well as K_m, a Michaelis constant, is the Michaelis-Menten model, one of the most widely used models in enzyme kinetics. The reaction scheme and formula describing the model are shown below:

$$\mathrm{E} + \mathrm{S} \underset{k_r}{\overset{k_f}{\rightleftharpoons}} \mathrm{ES} \xrightarrow{k_{\mathrm{cat}}} \mathrm{E} + \mathrm{P}$$

$$v = \frac{\mathrm{d}[\mathrm{P}]}{\mathrm{d}t} = V_{\max} \frac{[\mathrm{S}]}{K_{\mathrm{M}} + [\mathrm{S}]} = k_{\mathrm{cat}} [\mathrm{E}]_0 \frac{[\mathrm{S}]}{K_{\mathrm{M}} + [\mathrm{S}]}.$$

$$K_{\mathrm{M}} = \frac{k_r + k_{\mathrm{cat}}}{k_f}$$

A Michaelis-Menten graph is a plot describing the dependence of the initial reaction rate on the substrate concentration while keeping other parameters in the system constant. In order to plot a Michaelis-Menten graph, the initial rates (the enzymatic rate for the first 30 s) with varying substrate concentrations from 20 nM to 1000 nM (**Fig. 17**), were measured, and the values were reported in **Table 3**. Using the obtained data, the Michaelis-Menten graph was produced (**Fig. 18**). The general trend showed increased initial rates as substrate concentration rose until saturation at about [S] = 500 nM (**Table 3**). Increasing the substrate concentration past 500 nM did not significantly affect the reaction rate. The series was conducted in 5 mM and 10 mM of Mg^{2+}. Per our

expectations, a lower concentration of Mg^{2+} promoted a lower enzymatic activity. The Vmax of the ExoIII in 10 mM Mg^{2+} buffer reached 102.10 nM/min with a K_m of 272.5 nM (**Table 4**). Therefore, we report 12.76 nM/min as ExoIII's k_{cat} of a short DNA substrate freely floating in solution (**Table 4**).

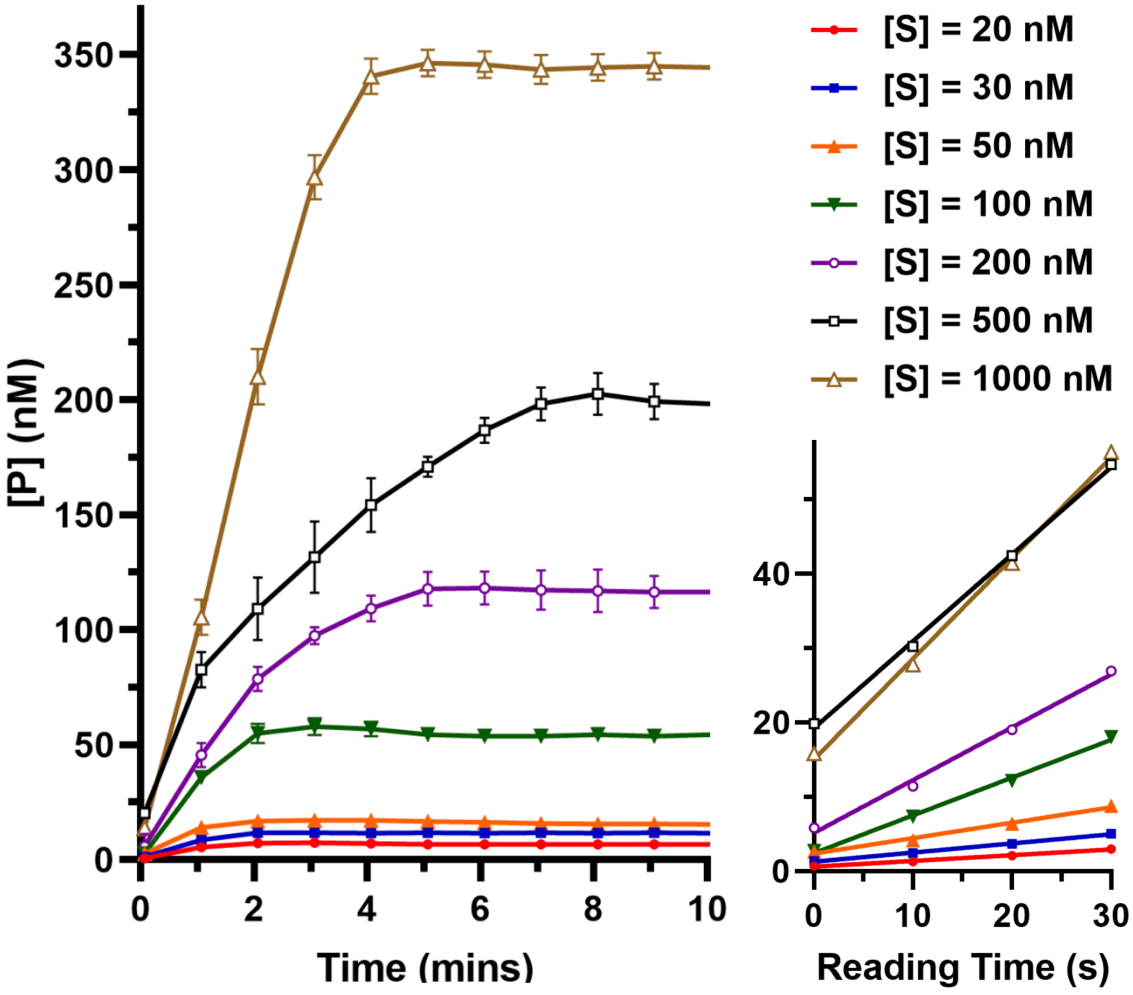

Figure 17. A range of the reactions between 8 nM of ExoIII and varying substrate concentrations. *Higher concentrations of the substrate resulted in the faster initial kinetic rates. For most of the reactions, saturation was reached when 30%-50% of the substrate*

was cleaved. An increase in the initial rates became smaller with using higher substrate concentrations. Doubling [S] from 500 nM to 1000 nM showed an almost negligent rise in the initial rate of the reaction.

Table 3. Initial rates of in-solution cleavage of ExoIII with a range of substrate concentrations.

[S]	Initial rate (first 30 s, Mg10)
20 nM	4.63 nM/min
30 nM	7.37 nM/min
50 nM	12.43 nM/min
100 nM	30.43 nM/min
200 nM	42.17 nM/min
500 nM	70.02 nM/min
1000 nM	77.52 nM/min

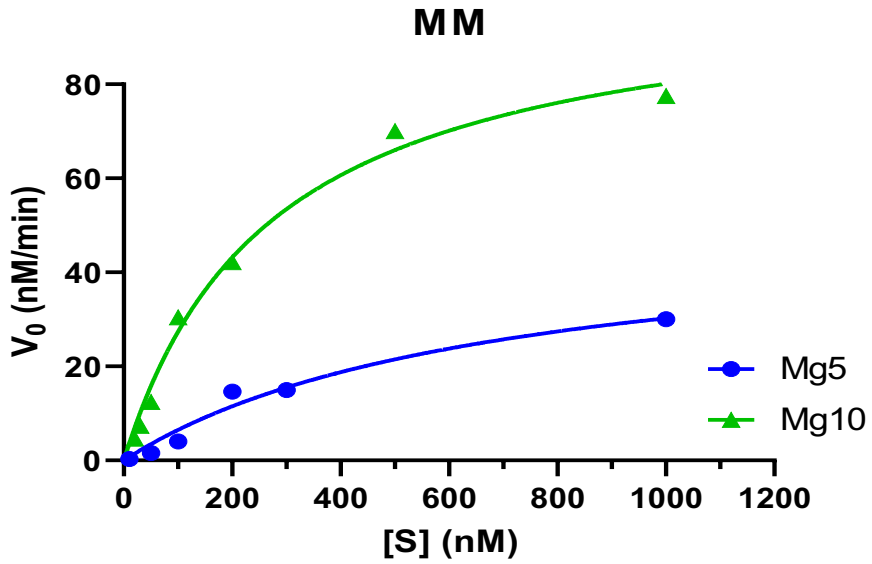

Figure 18. Michaelis-Menten plot of ExoIII's kinetic activity with varying Mg^{2+} concentrations. *The model demonstrates the initial rate of the enzymatic cleavage*

reaching a maximum of 50.92 nM/min for ExoIII in 5 mM Mg^{2+} solution, and a maximum of 102.10 nM/min in 10 mM Mg^{2+} solution. Per expectation, higher Mg^{2+} concentration leads to a higher reaction rate.

Table 4. Kinetic parameters of the in-solution cleavage of the substrate by ExoIII.

	Km	**Vmax**	**kcat**
With [Mg^{2+}] = 5 mM	685.4 nM	50.92 nM/min	6.36 min^{-1}
With [Mg^{2+}] = 10 mM	272.5 nM	102.10 nM/min	12.76 min^{-1}

Investigating ExoIII cleavage with PAGE gel electrophoresis

In-solution kinetic experiments described above provide crucial information regarding ExoIII's enzymatic potency and ability to interact with the DNA substrate. However, the biophysical properties and limitations of the enzymatic cleavage stay largely unaddressed with the kinetic assays. For this purpose, denaturing PAGE gel experiments were conducted. With this method's capability to decipher which strands of the annealed product get cleaved under what conditions, the urea PAGE gel runs carry important insights about ExoIII cleavage extent and selectivity. Indeed, the gel experiments revealed both expected results of the inhibition of the enzymatic activity with modified, protected DNA strands, and unexpected ones, particularly, of the existence of a barrier for cleavage created by the fluorescent dye.

ExoIII is an enzyme processively cleaving double-stranded DNA from both 3' ends of the substrate. In our experimental setup, this cleavage has to be directed to only one of the

3' ends of the fluorescently labeled substrate. Otherwise, the kinetic assays detecting the fluorescence intensity change due to the cleavage from only one end would become an inaccurate representation of the molecular process happening in reality. Moreover, cleavage from both 3' ends of DNA would mean an eventual consumption of the DNA legs of the particle in the rolling experiments.

To direct the cleavage of the enzyme to the 3' end of the Cy3-labeled fuel rather than the 3' end of gDNA – a desirable outcome for kinetic and rolling experiments – two types of protecting groups were employed on the 3' end of gDNA. First, a sequence of five thymines (T) was attached to the 3' end of gDNA in an attempt to create an unfavorable substrate recognition for ExoIII. Alternatively, the last nucleotide in the chain was flipped from 3' to 5' to effectively distract the ExoIII from starting the phosphodiester hydrolysis from this site. Original gDNA, gDNA with T5, and gDNA with an inverted nucleotide were tested along with their respective controls with either 8 nM or 40 nM of the enzyme (**Fig. 19**). The obtained gel was imaged with a general nucleic acid protocol to view the denatured remains of the reaction products as well as with a Cy3 filter to locate fluorescently active fuel strands.

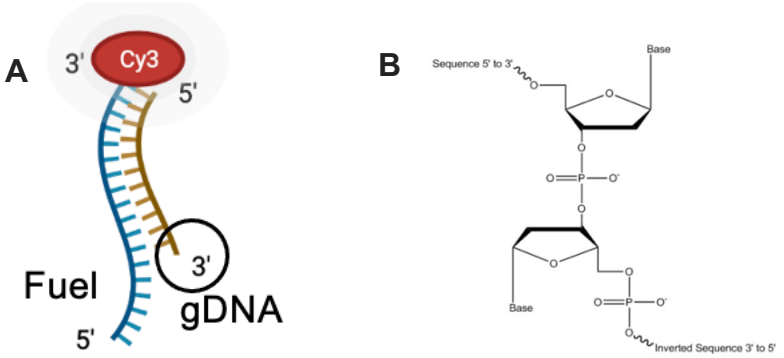

C

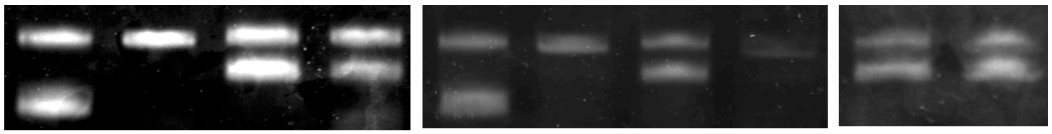

	1	2	3	4	5	6	7	8	9	10
Fuel(Cy3)	+	+	+	+	+	+	+	+	+	+
gDNA	+	+	-	-	+	+	-	-	+	-
gDNA-T5	-	-	+	+	-	-	+	+	-	-
Inv-gDNA*	-	-	-	-	-	-	-	-	-	+
ExoIII	-	8nM	-	8nM	-	40nM	-	40nM	-	40nM

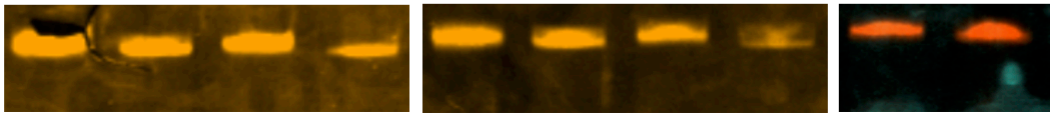

Figure 19. 20% urea PAGE gel study of the Cy3-labeled strand with varying ExoIII concentrations and protecting groups on the gDNA strand. A. *A schematic depicting the substrate investigated.* **B.** *An inverted nucleotide used as a protecting group in one of the gel runs.* **C.** *A palette demonstrating the observed DNA bands in the wells and the conditions per each well. Lanes 1, 3, 5, 7, and 9 serve as a control for the corresponding experimental condition. Lane 2 and 6 show cleavage of gDNA yet preservation of fuel after 8 nM or 40 nM ExoIII is added. Lane 4 show effective protection of gDNA by T5 sequence with 8 nM, yet Lane 8 depicts the loss of protection with higher concentrations*

of ExoIII. Lane 10 demonstrates the viability of the inverted nucleotide to protect gDNA. Preservation of the fuel strand in all wells, confirmed by the Cy3 filter imaging, points out the imposition of the barrier for cleavage by the Cy3 dye.

A closer look at the gel experiment with Cy3-labeled fuel reveals interesting and somewhat unexpected behavior of ExoIII (**Fig. 19**). First, 8 nM and 40 nM of ExoIII readily cleave the gDNA, as shown by the absence of gDNA bands in Lane 2 and Lane 6 compared to the control (Lane 1 and Lane 5). Lanes 3 and 4 turn out to be identical, meaning that the T5 sequence offers protection of the gDNA when 8 nM of ExoIII is added. However, once the concentration of the enzyme is increased to 40 nM, T5 is no longer an effective protection group (see Lanes 7 and 8). Lanes 9 and 10 show that an inverted nucleotide is also a potent protection, even in a reaction with 40 nM of ExoIII.

Unexpectedly, most of the fuel stayed preserved upon reacting with ExoIII. Imaging with a Cy3 filter confirmed the identity of the fuel strand in the gel. A likely reason for such behavior is a barrier that Cy3 imposes that protects the target 3' end from cleavage by ExoIII. This phenomenon was later confirmed by the on-surface kinetics experiments.

One of the general goals of the study was to measure the rate of the enzymatic cleavage of the DNA substrate by ExoIII. The inability of ExoIII to start cleavage from the 3' end due to Cy3 being a barrier suggested that an alternative experimental setup has to be imposed. For this reason, the Cy3 dye was replaced with the FAM dye, and the gel runs

with unprotected gDNA, T5-protected gDNA, and a gDNA with an inverted nucleotide were performed (**Fig. 20**).

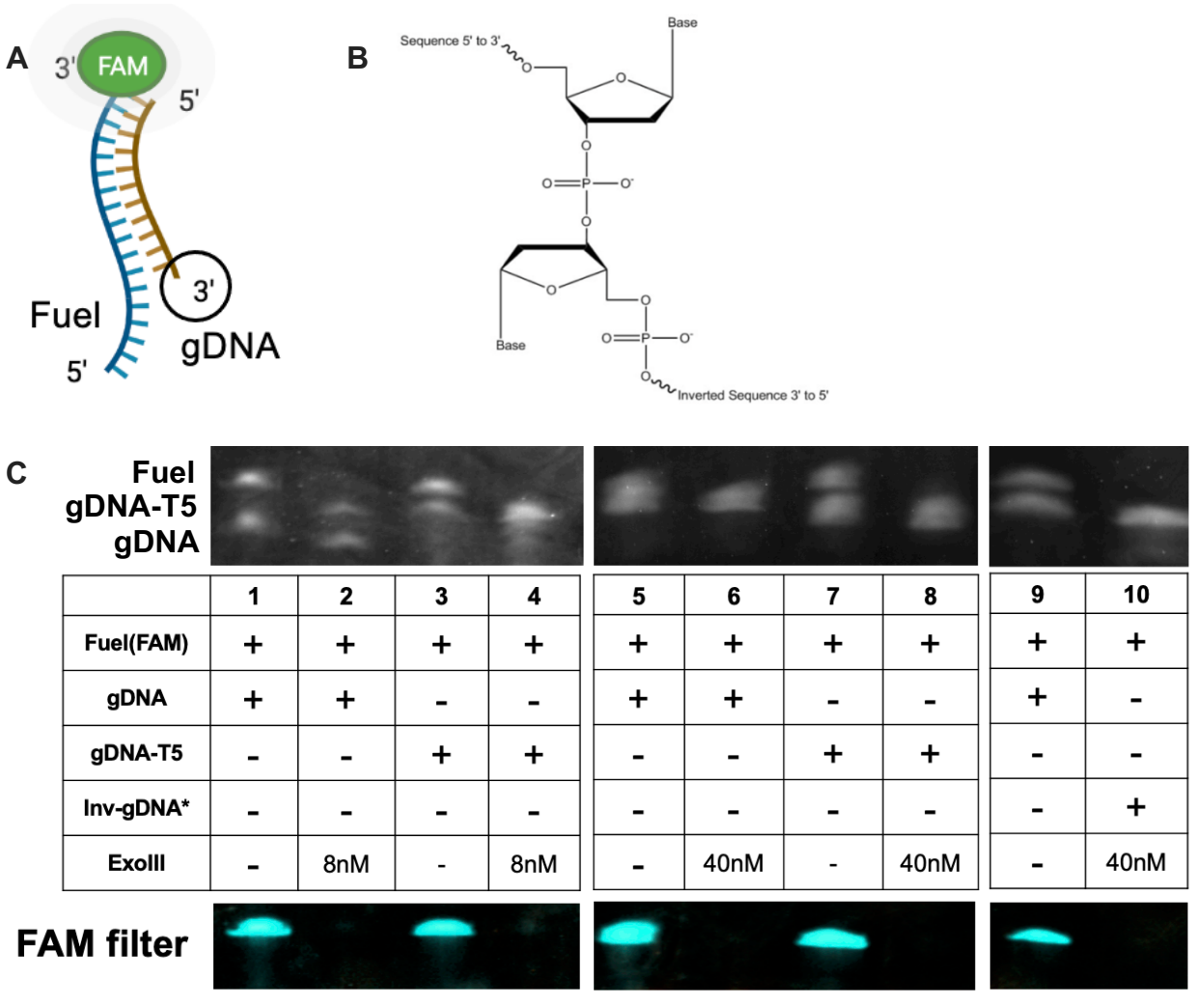

	1	2	3	4	5	6	7	8	9	10
Fuel(FAM)	+	+	+	+	+	+	+	+	+	+
gDNA	+	+	-	-	+	+	-	-	+	-
gDNA-T5	-	-	+	+	-	-	+	+	-	-
Inv-gDNA*	-	-	-	-	-	-	-	-	-	+
ExoIII	-	8nM	-	8nM	-	40nM	-	40nM	-	40nM

Figure 20. 20% urea PAGE gel study of the FAM-labeled strand with varying ExoIII concentrations and protecting groups on the gDNA strand. A. *A schematic depicting the substrate investigated.* **B.** *An inverted nucleotide used as a protecting group in one of the gel runs.* **C.** *A palette demonstrating the observed DNA bands in the wells and the conditions per each well. Lanes 1, 3, 5, 7, and 9 serve as a control for the corresponding experimental condition. Lane 2 and 6 show cleavage of gDNA after 8 nM or 40 nM ExoIII*

is added. Lane 4 and 8 show effective protection of gDNA by T5 sequence with 8 nM and 40 nM. Lane 10 demonstrates the viability of the inverted nucleotide to protect gDNA as well. Most importantly, all experimental wells showed an effective cleavage of the FAM-labeled fuel strand (confirmed by FAM-filter imaging), meaning that FAM barrier does not prevent ExoIII to access and hydrolyze bonds from the 3' end of the fuel strand.

Lanes 2 and 6 in **Fig. 20** showed enzymatic cleavage of both FAM-labeled fuel and, to a lesser extent, of the unprotected gDNA. The addition of T5 protected gDNA from both 8 nM and 40 nM of ExoIII compared to the controls (Lanes 3-4, 7-8). The inverted nucleotide protected gDNA from high concentrations of ExoIII, while a fuel strand was getting cleaved by ExoIII. FAM filter demonstrated the presence of FAM-labeled substrate in the controls but the absence of it in the reacted sample (**Fig. 20**). Overall, these gel studies showed that the usage of T5 or inverted nucleotides as protecting groups together with a FAM fuel deliver the most desirable outcomes for the subsequent on-surface experimentation.

On-surface kinetic assay setup

'A third part of this study was to investigate the ExoIII's behavior with substrates immobilized on the surface. An answer to this fundamental question would allow us to make a qualitative relation between the enzyme kinetics in two environments, as well as become a milestone in the creation of the ExoIII's powered DNA rolling motors. For this purpose, a previously mentioned experimental setup was redesigned and shown in Fig. X. Unlike the in-solution assay where the enzyme cleaved the 3' end with an attached

BHQ2 quencher, this time, a Cy3 fluorophore was attached to the fuel's strand and reacted with the enzyme. The system was hydrolyzed with the DNA anchor immobilized on the glass surface. Per our setup, the cleavage of the 3' end with a fluorophore would result in the signal depletion of the surface detected by the microscope. At least three replicates of each microscope capture were conducted, and fluorescence intensity was later normalized to elucidate the rate of cleavage of the substrate by the ExoIII.

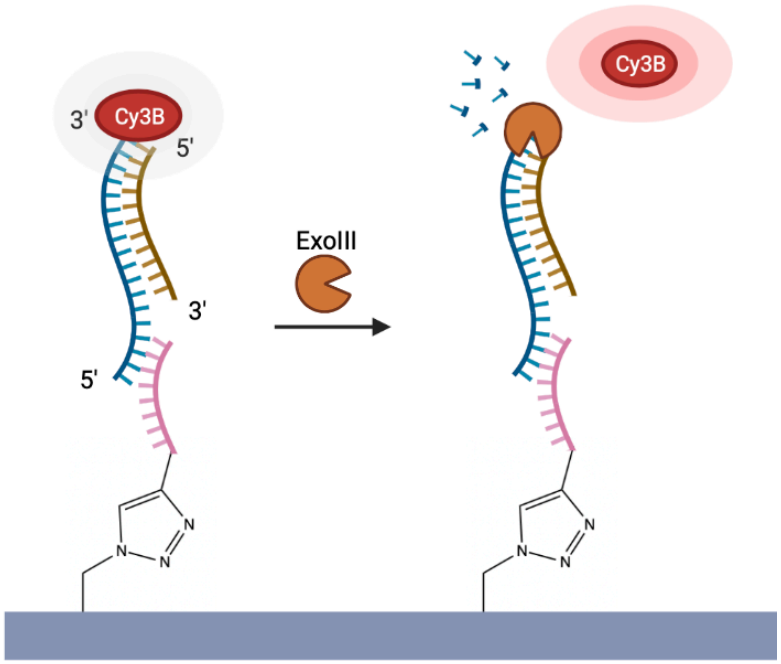

Figure 21. A scheme of the on-surface kinetic assay design. *An assay with a Cy3-modified fuel strand was used to obtain the on-surface k_{cat} of ExoIII.*

Confirmation of ExoIII's inability to cleave a Cy3-labeled end

The proposed experimental design resulted in a slow and non-processive cleavage of the substrate on the surface. This inference was made when observing a minimal, negligible Cy3 signal depletion after the immobilized substrate was treated with 40 nM of the ExoIII for 20 mins (**Fig. 21**). The change in the fluorescence intensity was accrued mainly due to the photobleaching. A positive control trial with a fifty-fold higher concentration of the ExoIII (2000 nM) showed a considerable signal depletion (over 40% of the substrate was cleaved in 20 mins). This experiment confirms the failure of ExoIII to cleave the substrate from the 3'-end labeled with the Cy3 that was previously reported in the PAGE gel studies.

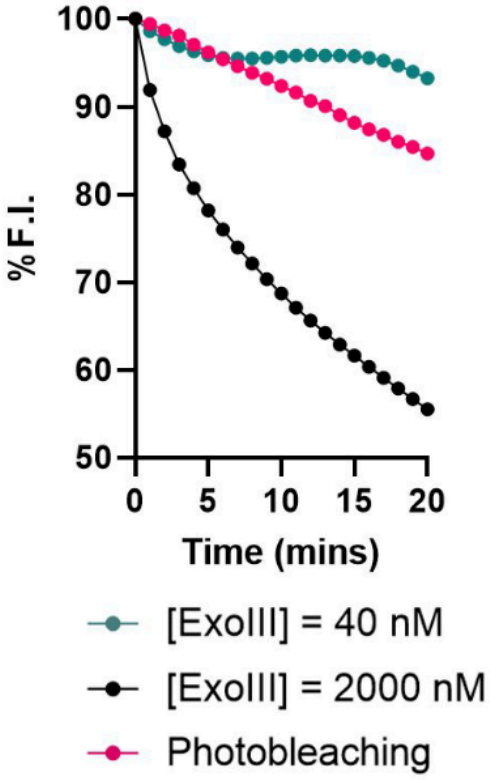

Figure 21. A surface depletion experiment confirming ExoIII's failed cleavage of Cy3-modified fuel strand. *The addition of 40 nM of ExoIII to the surface-bound Cy3-modified fuel strand did not result in a significant signal depletion. The drop in the relative fluorescence intensity was largely due to the photobleaching. A positive control with the fifty-fold higher enzymatic concentration demonstrated significant Cy3 signal depletion.*

Redesign of on-surface kinetic assay setup

To solve the issue of the Cy3 serving as a barrier for enzymatic cleavage, a different fluorescent dye (FAM) was chosen to measure the k_{cat} (**Fig. 22**). Earlier, the PAGE gel study showed that the FAM-labeled fuel strand was getting processively cleaved by both 8 nM and 40 nM of the ExoIII (Fig. X). An updated experimental design also included the Cy5 dye on the 3' end of the gDNA. The Cy5-modified gDNA was used for two reasons:

(1) as a protecting group from the ExoIII's cleavage, (2) as a fluorophore used in determining the koff of the system. The PAGE gel electrophoresis had shown viable protection of the gDNA with a Cy5 dye on par with the protection given by the T5 sequence or an inverted nucleotide. The koff measurement was accounted for due to a likely lag between the rate of the enzymatic cleavage and a complete unbinding of the gDNA from the fuel strand. Therefore, the Cy5 signal depletion on the surface would indicate the actual rate of the gDNA unzipping from the complementary strand due to the enzymatic cleavage. In the end, the new on-surface kinetic assay solved the issue with a non-cleavage of a fluorescently labeled fuel strand, put an extra protecting group on the 3' end of gDNA, and offered a chance to measure not only the k_{cat} but also the k_{off} rate.

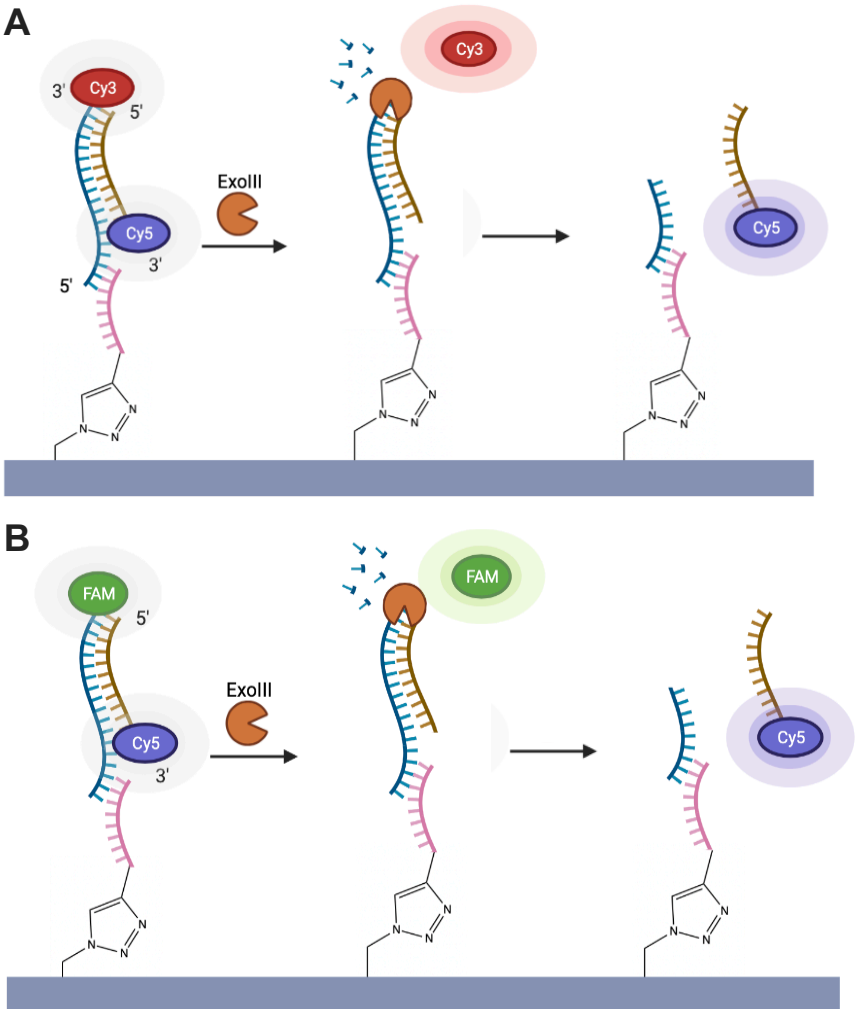

Figure 22. A scheme of the redesigned on-surface kinetic assay design. ***A.*** *An assay with a Cy3-modified fuel strand and a Cy5-modified gDNA was used to detect the on-surface* k_{cat} *and* k_{off} *of ExoIII.* ***B.*** *An assay with a FAM-modified fuel strand and a Cy5-modified gDNA was used to detect the on-surface* k_{cat} *and* k_{off} *of ExoIII.*

Verifying ExoIII interaction with new design

ExoIII interaction with a substrate of a new design was tested using denaturing PAGE gel electrophoresis (**Fig. 23**). FAM-labeled fuel and Cy5-labeled gDNA were annealed and reacted with either 8 nM or 40 nM of ExoIII, subsequent results imaged with FAM

and Cy5 combined filter are shown in Lanes 2 and 4 of **Fig. 23**. It is clear that with either enzyme concentrations, the FAM-labeled fuel undergoes cleavage while Cy5-labeled gDNA is protected by Cy5 and, presumably, an addition sequence of 5T on its 3' end. The gel confirms the utility of the proposed design to direct enzymatic cleavage towards the 3' end of the fuel for the purposes of the kinetic assay.

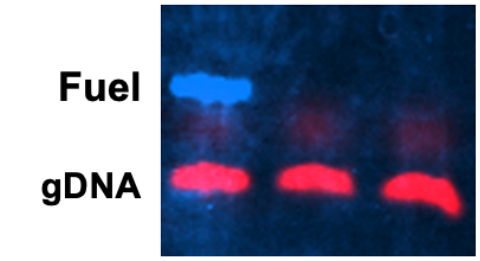

	1	2	3
Fuel(FAM)	+	+	+
gDNA-Cy5	+	+	+
ExoIII	-	8nM	40nM

Figure 23. 20% urea PAGE gel study of the FAM-labeled strand and Cy5-labeled gDNA with varying ExoIII concentrations. *A palette demonstrating the observed DNA bands in the wells and the conditions per each well. Lanes 1 serves as a control for the corresponding experimental condition with both fuel and gDNA present when no enzyme was added. Lanes 2 and 3 show cleavage of FAM-fuel after either 8 nM or 40 nM of ExoIII in the solution. gDNA band stays intact in Lanes 2 and 3, meaning that gDNA is protected against enzymatic cleavage under both conditions.*

Obtaining on-surface k_{cat} and k_{off} rates

Two types of substrate strands (FAM-labeled and Cy3-labeled) were hybridized to the DNA anchor strand according to the experimental setup described above. Then, gDNA conjugated with the Cy5 dye was added. Each type of substrate was treated with either 8 nM or 40 nM of the ExoIII, and the surface signal depletion was recorded every ten minutes. Neither 8 nM nor 40 nM seemed to cause significant depletion of the Cy3 or Cy5 signal and, thus, showing slow k_{cat} and k_{off} rates (**Fig. 24**). As seen before, this phenomenon confirms the inability of the ExoIII to access the 3' end of the fuel strand and start processive cleavage. This failure to cleave the fuel, in turn, results in the preservation of gDNA being annealed to the fuel.

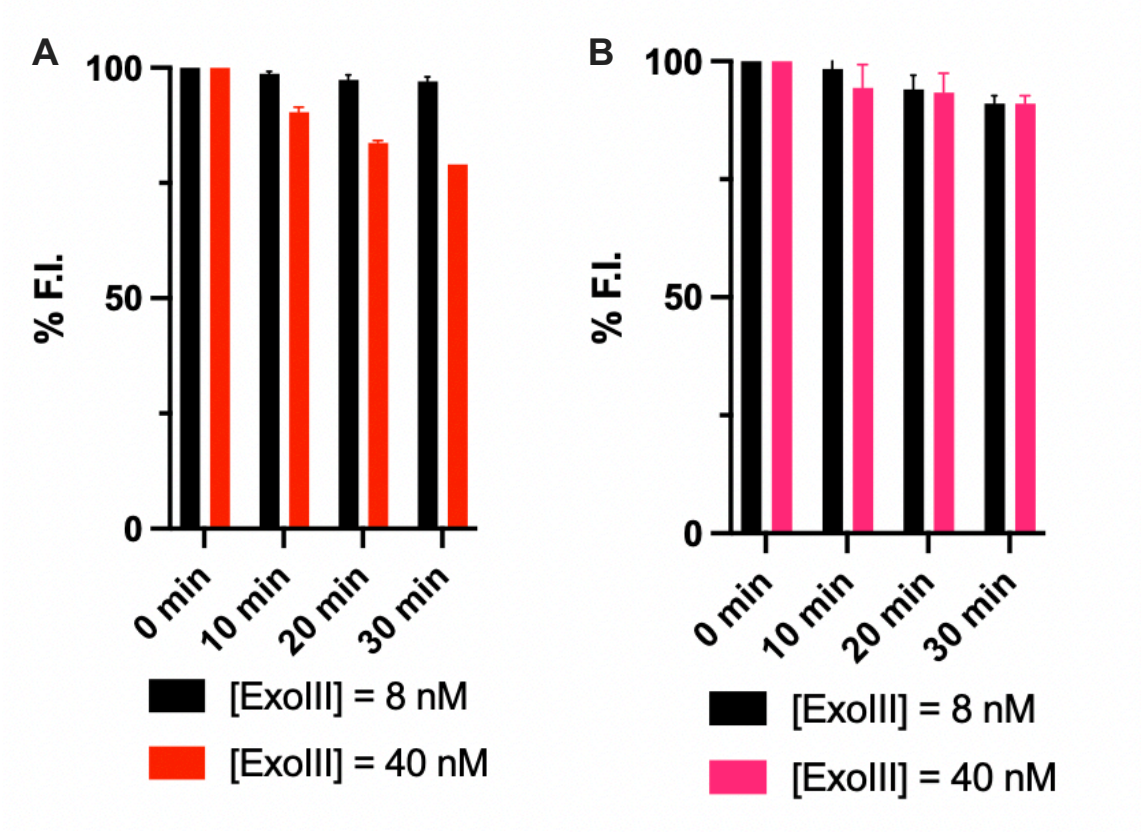

Figure 24. Cy3 and Cy5 signal depletion with 8 nM and 40 nM of ExoIII. *Reactions with both 8 nM and 40 nM of ExoIII do not show a significant Cy3 and Cy5 signal depletion, confirming the inability of ExoIII to access and cleave the Cy3-modified fuel strand.* ***A.*** *FAM signal depleted due to the cleavage of the FAM-modified fuel strand, with the rate indicating the* k_{cat} *of ExoIII.* ***B.*** *Cy5 signal depleted due to the unbinding of a Cy5-modified gDNA as a result of the enzymatic cleavage of the fuel strand, with the rate indicating the* k_{off} *of ExoIII.*

In contrast, when the FAM-labeled fuel is used, the enzymatic cleavage proceeds further and both FAM and Cy5 signal get depleted (**Fig. 25**). Per our expectations, higher concentrations of the ExoIII result in faster and stronger depletion. For most of the substrates, the reaction reaches saturation after 10 mins. 8 nM of ExoIII give the V_{cat} of the ExoIII in this condition is 2.1 nM/min and V_{off} of the ExoIII is 1.6 nM/min. 40 nM of ExoIII show V_{cat} of 3.9 nM/min and V_{off} of 2.6 nM/min. Therefore, the k_{cat} of ExoIII with surface-immobilized substrates is 0.1-0.3 min^{-1}, while the k_{off} of the substate in the system is 0.1-0.2 min^{-1}. The reaction rates of the ExoIII with a surface-bound substrate are slower than those in the free-floating system (k_{cat} = 12.8 min^{-1}), likely due to steric unavailability of the cleavage site, limited molecular collisions between the enzyme and substrate, and higher rigidity of the structural conformation of the DNA attached to the surface.

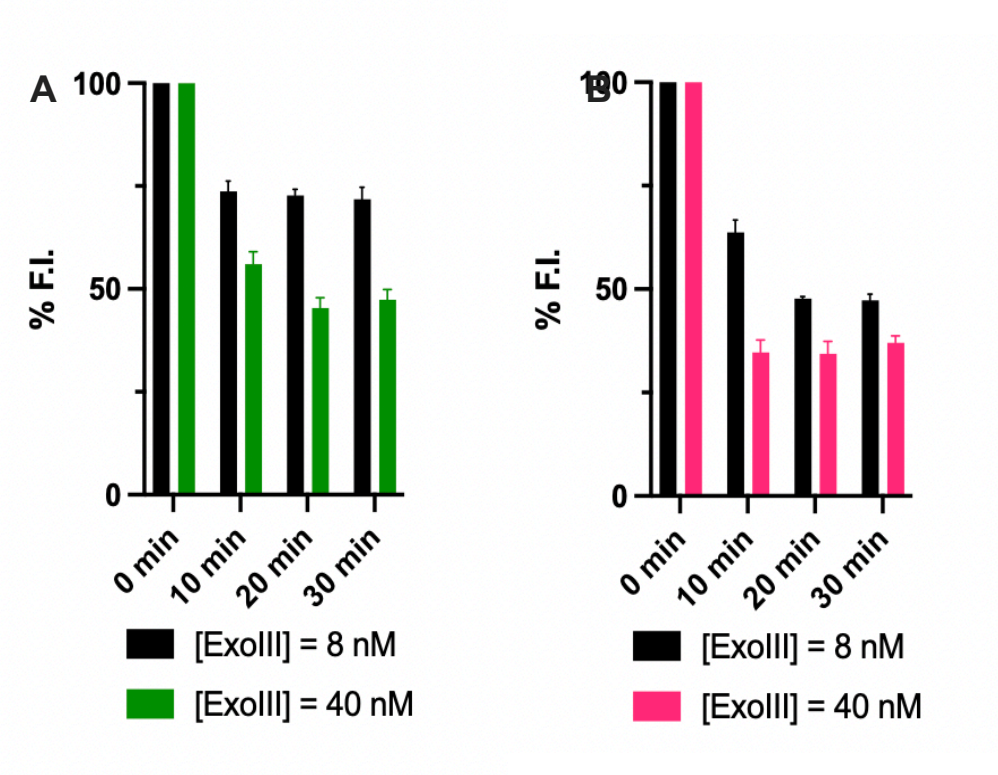

Figure 25. FAM and Cy5 signal depletion with 8 nM and 40 nM of ExoIII. *Reactions with a higher enzyme concentration result in a steeper signal depletion. Most of reactions are completed after 10 mins.* ***A.*** *FAM signal depleted due to the cleavage of the FAM-modified fuel strand, with the rate indicating the* k_{cat} *of ExoIII.* ***B.*** *Cy5 signal depleted due to the unbinding of a Cy5-modified gDNA as a result of the enzymatic cleavage of the fuel strand, with the rate indicating the* k_{off} *of ExoIII.*

Conclusion and Future Directions

At the beginning of this study, we have set three distinct goals: (1) elucidating the fundamental knowledge of the kinetics of ExoIII, (2) identifying optimal parameters for the enzymatic cleavage, (3) contributing to the RNA-free rolling motor project devised by Yusha Imtiaz. In general, the study has succeeded in addressing all three goals. Firstly, the cleavage rates of ExoIII interacting with the substrate in solution (k_{cat} = 12.76 min^{-1}) and on surface (k_{cat} = 0.1-0.3 min^{-1}, and k_{off} = 0.1-0.2 min^{-1}) were reported. The basic relation between kinetic constants shows a significant role in the surrounding environment on the processivity of cleavage. According to the second goal, numerous conditions were tested and analyzed to develop the most optimal workflow and conditions for successful enzyme on-surface assays and rolling experiments. Lastly, the obtained data, for example, of the Cy3 barrier against the ExoIII, have aided the progress of the ExoIII-powered motors.

A logical future direction of the project is to measure the kinetics of the enzyme-substrate interaction with the rolling beads present. Another exciting field of exploration is to test different DNA sequences and GC content as the fuel and gDNA, use asymmetric DNA strands, and measure the rates of those enzymatic reactions. A research design can also be expanded to other enzymes such as RNase H or ExoI. However, the most promising and groundbreaking approach to undertake what seems to be an original large project of constructing the DNA rolling motors using ExoIII. It is with great hope and anticipation we work toward further development of the variety of nanomachines, including DNA rolling motors, for their applications in technology and medicine of tomorrow.

References

(1) Yan, K.; Gao, L.-N.; Cui, Y.-L.; Zhang, Y.; Zhou, X. The Cyclic AMP Signaling Pathway: Exploring Targets for Successful Drug Discovery (Review). *Mol. Med. Rep.* **2016**, *13* (5), 3715–3723. https://doi.org/10.3892/mmr.2016.5005.

(2) Mor, I.; Cheung, E. C.; Vousden, K. H. Control of Glycolysis through Regulation of PFK1: Old Friends and Recent Additions. *Cold Spring Harb. Symp. Quant. Biol.* **2011**, *76* (0), 211–216. https://doi.org/10.1101/sqb.2011.76.010868.

(3) Moriyama, T.; Sato, N. Enzymes Involved in Organellar DNA Replication in Photosynthetic Eukaryotes. *Front. Plant Sci.* **2014**, *5*. https://doi.org/10.3389/fpls.2014.00480.

(4) Walter, N. G.; Engelke, D. R. Ribozymes: Catalytic RNAs That Cut Things, Make Things, and Do Odd and Useful Jobs. *Biol. Lond. Engl.* **2002**, *49* (5), 199–203.

(5) Espina, G.; Atalah, J.; Blamey, J. M. Extremophilic Oxidoreductases for the Industry: Five Successful Examples With Promising Projections. *Front. Bioeng. Biotechnol.* **2021**, *9*, 710035. https://doi.org/10.3389/fbioe.2021.710035.

(6) Martínez Cuesta, S.; Rahman, S. A.; Thornton, J. M. Exploring the Chemistry and Evolution of the Isomerases. *Proc. Natl. Acad. Sci.* **2016**, *113* (7), 1796–1801. https://doi.org/10.1073/pnas.1509494113.

(7) Shukla, E.; D. Bendre, A.; M. Gaikwad, S. Hydrolases: The Most Diverse Class of Enzymes. In *Biochemistry*; Haider, S., Haider, A., Catalá, A., Eds.; IntechOpen, 2022; Vol. 29. https://doi.org/10.5772/intechopen.102350.

(8) López-Otín, C.; Bond, J. S. Proteases: Multifunctional Enzymes in Life and Disease. *J. Biol. Chem.* **2008**, *283* (45), 30433–30437. https://doi.org/10.1074/jbc.R800035200.

(9) Hou, C. T.; Shimada, Y. Lipases. In *Encyclopedia of Microbiology*; Elsevier, 2009; pp 385–392. https://doi.org/10.1016/B978-012373944-5.00153-X.

(10) Amin, K.; Tranchimand, S.; Benvegnu, T.; Abdel-Razzak, Z.; Chamieh, H. Glycoside Hydrolases and Glycosyltransferases from Hyperthermophilic Archaea: Insights on Their Characteristics and Applications in Biotechnology. *Biomolecules* **2021**, *11* (11), 1557. https://doi.org/10.3390/biom11111557.

(11) Santa, P.; Garreau, A.; Serpas, L.; Ferriere, A.; Blanco, P.; Soni, C.; Sisirak, V. The Role of Nucleases and Nucleic Acid Editing Enzymes in the Regulation of Self-Nucleic Acid Sensing. *Front. Immunol.* **2021**, *12*, 629922. https://doi.org/10.3389/fimmu.2021.629922.

(12) Yang, W. Nucleases: Diversity of Structure, Function and Mechanism. *Q. Rev. Biophys.* **2011**, *44* (1), 1–93. https://doi.org/10.1017/S0033583510000181.

(13) Mol, C. D.; Kuo, C.-F.; Thayer, M. M.; Cunningham, R. P.; Tainer, J. A. Structure and Function of the Multifunctional DNA-Repair Enzyme Exonuclease III. *Nature* **1995**, *374* (6520), 381–386. https://doi.org/10.1038/374381a0.

(14) Hackett, P. B.; Somia, N. V. Delivering the Second Revolution in Site-Specific Nucleases. *eLife* **2014**, *3*, e02904. https://doi.org/10.7554/eLife.02904.

(15) Yang, W. Topoisomerases and Site-Specific Recombinases: Similarities in Structure and Mechanism. *Crit. Rev. Biochem. Mol. Biol.* **2010**, *45* (6), 520–534. https://doi.org/10.3109/10409238.2010.513375.
(16) Samejima, K.; Earnshaw, W. C. Trashing the Genome: The Role of Nucleases during Apoptosis. *Nat. Rev. Mol. Cell Biol.* **2005**, *6* (9), 677–688. https://doi.org/10.1038/nrm1715.
(17) Salgia, S. R.; Singh, S. K.; Gurha, P.; Gupta, R. Two Reactions of Haloferax Volcanii RNA Splicing Enzymes: Joining of Exons and Circularization of Introns. *RNA N. Y. N* **2003**, *9* (3), 319–330. https://doi.org/10.1261/rna.2118203.
(18) Mason, P. A.; Cox, L. S. The Role of DNA Exonucleases in Protecting Genome Stability and Their Impact on Ageing. *Age Dordr. Neth.* **2012**, *34* (6), 1317–1340. https://doi.org/10.1007/s11357-011-9306-5.
(19) Lovett, S. T. The DNA Exonucleases of *Escherichia Coli*. *EcoSal Plus* **2011**, *4* (2), ecosalplus.4.4.7. https://doi.org/10.1128/ecosalplus.4.4.7.
(20) Zuo, Y.; Zheng, H.; Wang, Y.; Chruszcz, M.; Cymborowski, M.; Skarina, T.; Savchenko, A.; Malhotra, A.; Minor, W. Crystal Structure of RNase T, an Exoribonuclease Involved in TRNA Maturation and End Turnover. *Struct. Lond. Engl. 1993* **2007**, *15* (4), 417–428. https://doi.org/10.1016/j.str.2007.02.004.
(21) Takahashi, S.; Usui, T.; Kawasaki, S.; Miyata, H.; Kurita, H.; Matsuura, S.; Mizuno, A.; Oshige, M.; Katsura, S. Real-Time Single-Molecule Observations of T7 Exonuclease Activity in a Microflow Channel. *Anal. Biochem.* **2014**, *457*, 24–30. https://doi.org/10.1016/j.ab.2014.04.012.
(22) Werner, J. H.; Cai, H.; Keller, R. A.; Goodwin, P. M. Exonuclease I Hydrolyzes DNA with a Distribution of Rates. *Biophys. J.* **2005**, *88* (2), 1403–1412. https://doi.org/10.1529/biophysj.104.044255.
(23) Breyer, W. A.; Matthews, B. W. A Structural Basis for Processivity. *Protein Sci. Publ. Protein Soc.* **2001**, *10* (9), 1699–1711. https://doi.org/10.1110/ps.10301.
(24) Schultz, S. J.; Champoux, J. J. RNase H Activity: Structure, Specificity, and Function in Reverse Transcription. *Virus Res.* **2008**, *134* (1–2), 86–103. https://doi.org/10.1016/j.virusres.2007.12.007.
(25) *Properties of Exonucleases and Non-specific Endonucleases | NEB*. https://www.neb.com/tools-and-resources/selection-charts/properties-of-exonucleases-and-nonspecific-endonucleases (accessed 2023-03-16).
(26) Black, C. B.; Cowan, J. A. Inert Chromium and Cobalt Complexes as Probes of Magnesium-Dependent Enzymes. Evaluation of the Mechanistic Role of the Essential Metal Cofactor in Escherichia Coli Exonuclease III. *Eur. J. Biochem.* **1997**, *243* (3), 684–689. https://doi.org/10.1111/j.1432-1033.1997.00684.x.
(27) Yang, L.; Arora, K.; Beard, W. A.; Wilson, S. H.; Schlick, T. Critical Role of Magnesium Ions in DNA Polymerase β's Closing and Active Site Assembly. *J. Am. Chem. Soc.* **2004**, *126* (27), 8441–8453. https://doi.org/10.1021/ja049412o.
(28) Sissi, C.; Palumbo, M. Effects of Magnesium and Related Divalent Metal Ions in Topoisomerase Structure and Function. *Nucleic Acids Res.* **2009**, *37* (3), 702–711. https://doi.org/10.1093/nar/gkp024.
(29) Bank, R. P. D. *RCSB PDB - 1AKO: EXONUCLEASE III FROM ESCHERICHIA COLI*. https://www.rcsb.org/structure/1ako (accessed 2023-03-16).

(30) *Exonuclease III (E. coli)* | *NEB*. https://www.neb.com/products/m0206-exonuclease-iii-e-coli#Product%20Information (accessed 2023-03-16).
(31) Borrego-Soto, G.; Ortiz-López, R.; Rojas-Martínez, A. Ionizing Radiation-Induced DNA Injury and Damage Detection in Patients with Breast Cancer. *Genet. Mol. Biol.* **2015**, *38* (4), 420–432. https://doi.org/10.1590/S1415-475738420150019.
(32) Shida, T.; Kaneda, K.; Ogawa, T.; Sekiguchi, J. Abasic Site Recognition Mechanism by the Escherichia Coli Exonuclease III. *Nucleic Acids Symp. Ser.* **1999**, *42* (1), 195–196. https://doi.org/10.1093/nass/42.1.195.
(33) Henikoff, S. Unidirectional Digestion with Exonuclease III Creates Targeted Breakpoints for DNA Sequencing. *Gene* **1984**, *28* (3), 351–359. https://doi.org/10.1016/0378-1119(84)90153-7.
(34) Slatko, B.; Heinrich, P.; Nixon, B. T.; Voytas, D. Constructing Nested Deletions for Use in DNA Sequencing. *Curr. Protoc. Mol. Biol.* **1991**, *16* (1). https://doi.org/10.1002/0471142727.mb0702s16.
(35) Barzilay, G.; Walker, L. J.; Robson, C. N.; Hickson, I. D. Site-Directed Mutagenesis of the Human DNA Repair Enzyme HAP1: Identification of Residues Important for AP Endonuclease and RNase H Activity. *Nucleic Acids Res.* **1995**, *23* (9), 1544–1550. https://doi.org/10.1093/nar/23.9.1544.
(36) Sheyitov, B.; Imtiaz, Y.; Bazrafshan, A.; Salaita, K. Investigating Optimal Kinetic Parameters of Exonuclease III to Create a Next-Generation, Robust, Self-Avoiding Rolling Motor Biosensor. *Biophys. J.* **2023**, *122* (3), 437a. https://doi.org/10.1016/j.bpj.2022.11.2359.
(37) Baroncini, M.; Casimiro, L.; de Vet, C.; Groppi, J.; Silvi, S.; Credi, A. Making and Operating Molecular Machines: A Multidisciplinary Challenge. *ChemistryOpen* **2018**, *7* (2), 169–179. https://doi.org/10.1002/open.201700181.
(38) Yoshida, M.; Muneyuki, E.; Hisabori, T. ATP Synthase — a Marvellous Rotary Engine of the Cell. *Nat. Rev. Mol. Cell Biol.* **2001**, *2* (9), 669–677. https://doi.org/10.1038/35089509.
(39) Cochran, J. C.; Kull, F. J. Kinesin Motors: No Strain, No Gain. *Cell* **2008**, *134* (6), 918–919. https://doi.org/10.1016/j.cell.2008.09.005.
(40) Makarova, T. M.; Bogdanov, A. A. The Ribosome as an Allosterically Regulated Molecular Machine. *Biochem. Mosc.* **2017**, *82* (13), 1557–1571. https://doi.org/10.1134/S0006297917130016.
(41) Sengupta, S.; Spiering, M. M.; Dey, K. K.; Duan, W.; Patra, D.; Butler, P. J.; Astumian, R. D.; Benkovic, S. J.; Sen, A. DNA Polymerase as a Molecular Motor and Pump. *ACS Nano* **2014**, *8* (3), 2410–2418. https://doi.org/10.1021/nn405963x.
(42) Whitehouse, D. G.; May, B.; Moore, A. L. Respiratory Chain and ATP Synthase. In *Reference Module in Biomedical Sciences*; Elsevier, 2019; p B9780128012383957000. https://doi.org/10.1016/B978-0-12-801238-3.95732-5.
(43) Neupane, P.; Bhuju, S.; Thapa, N.; Bhattarai, H. K. ATP Synthase: Structure, Function and Inhibition. *Biomol. Concepts* **2019**, *10* (1), 1–10. https://doi.org/10.1515/bmc-2019-0001.
(44) Hirokawa, N.; Noda, Y.; Tanaka, Y.; Niwa, S. Kinesin Superfamily Motor Proteins and Intracellular Transport. *Nat. Rev. Mol. Cell Biol.* **2009**, *10* (10), 682–696. https://doi.org/10.1038/nrm2774.

(45) Canty, J. T.; Tan, R.; Kusakci, E.; Fernandes, J.; Yildiz, A. Structure and Mechanics of Dynein Motors. *Annu. Rev. Biophys.* **2021**, *50*, 549–574. https://doi.org/10.1146/annurev-biophys-111020-101511.
(46) Wulf, S. F.; Ropars, V.; Fujita-Becker, S.; Oster, M.; Hofhaus, G.; Trabuco, L. G.; Pylypenko, O.; Sweeney, H. L.; Houdusse, A. M.; Schröder, R. R. Force-Producing ADP State of Myosin Bound to Actin. *Proc. Natl. Acad. Sci.* **2016**, *113* (13). https://doi.org/10.1073/pnas.1516598113.
(47) Dimitrova-Paternoga, L.; Jagtap, P. K. A.; Cyrklaff, A.; Vaishali, null; Lapouge, K.; Sehr, P.; Perez, K.; Heber, S.; Löw, C.; Hennig, J.; Ephrussi, A. Molecular Basis of MRNA Transport by a Kinesin-1-Atypical Tropomyosin Complex. *Genes Dev.* **2021**, *35* (13–14), 976–991. https://doi.org/10.1101/gad.348443.121.
(48) Toprak, E.; Yildiz, A.; Hoffman, M. T.; Rosenfeld, S. S.; Selvin, P. R. Why Kinesin Is so Processive. *Proc. Natl. Acad. Sci.* **2009**, *106* (31), 12717–12722. https://doi.org/10.1073/pnas.0808396106.
(49) Roke, D.; Wezenberg, S. J.; Feringa, B. L. Molecular Rotary Motors: Unidirectional Motion around Double Bonds. *Proc. Natl. Acad. Sci.* **2018**, *115* (38), 9423–9431. https://doi.org/10.1073/pnas.1712784115.
(50) Shi, M.; Yeatman, E. M. A Comparative Review of Artificial Muscles for Microsystem Applications. *Microsyst. Nanoeng.* **2021**, *7* (1), 95. https://doi.org/10.1038/s41378-021-00323-5.
(51) Silvi, S.; Venturi, M.; Credi, A. Artificial Molecular Shuttles: From Concepts to Devices. *J. Mater. Chem.* **2009**, *19* (16), 2279. https://doi.org/10.1039/b818609j.
(52) Leigh, D. A.; Lewandowska, U.; Lewandowski, B.; Wilson, M. R. Synthetic Molecular Walkers. In *Molecular Machines and Motors*; Credi, A., Silvi, S., Venturi, M., Eds.; Topics in Current Chemistry; Springer International Publishing: Cham, 2014; Vol. 354, pp 111–138. https://doi.org/10.1007/128_2014_546.
(53) Cheng, C.; McGonigal, P. R.; Schneebeli, S. T.; Li, H.; Vermeulen, N. A.; Ke, C.; Stoddart, J. F. An Artificial Molecular Pump. *Nat. Nanotechnol.* **2015**, *10* (6), 547–553. https://doi.org/10.1038/nnano.2015.96.
(54) Erbas-Cakmak, S.; Leigh, D. A.; McTernan, C. T.; Nussbaumer, A. L. Artificial Molecular Machines. *Chem. Rev.* **2015**, *115* (18), 10081–10206. https://doi.org/10.1021/acs.chemrev.5b00146.
(55) Carroll, W. R.; Zhao, C.; Smith, M. D.; Pellechia, P. J.; Shimizu, K. D. A Molecular Balance for Measuring Aliphatic CH-π Interactions. *Org. Lett.* **2011**, *13* (16), 4320–4323. https://doi.org/10.1021/ol201657p.
(56) Simpson, C. D.; Mattersteig, G.; Martin, K.; Gherghel, L.; Bauer, R. E.; Räder, H. J.; Müllen, K. Nanosized Molecular Propellers by Cyclodehydrogenation of Polyphenylene Dendrimers. *J. Am. Chem. Soc.* **2004**, *126* (10), 3139–3147. https://doi.org/10.1021/ja036732j.
(57) Simpson, G. J.; García-López, V.; Petermeier, P.; Grill, L.; Tour, J. M. How to Build and Race a Fast Nanocar. *Nat. Nanotechnol.* **2017**, *12* (7), 604–606. https://doi.org/10.1038/nnano.2017.137.
(58) Gil-Ramírez, G.; Leigh, D. A.; Stephens, A. J. Catenanes: Fifty Years of Molecular Links. *Angew. Chem. Int. Ed.* **2015**, *54* (21), 6110–6150. https://doi.org/10.1002/anie.201411619.

(59) Ramezani, H.; Dietz, H. Building Machines with DNA Molecules. *Nat. Rev. Genet.* **2020**, *21* (1), 5–26. https://doi.org/10.1038/s41576-019-0175-6.
(60) Fadler, R. E.; Flood, A. H. Rigidity and Flexibility in Rotaxanes and Their Relatives; On Being Stubborn and Easy-Going. *Front. Chem.* **2022**, *10*, 856173. https://doi.org/10.3389/fchem.2022.856173.
(61) Feringa, B. L. The Art of Building Small: From Molecular Switches to Motors (Nobel Lecture). *Angew. Chem. Int. Ed.* **2017**, *56* (37), 11060–11078. https://doi.org/10.1002/anie.201702979.
(62) Erbas-Cakmak, S.; Fielden, S. D. P.; Karaca, U.; Leigh, D. A.; McTernan, C. T.; Tetlow, D. J.; Wilson, M. R. Rotary and Linear Molecular Motors Driven by Pulses of a Chemical Fuel. *Science* **2017**, *358* (6361), 340–343. https://doi.org/10.1126/science.aao1377.
(63) von Delius, M.; Geertsema, E. M.; Leigh, D. A. A Synthetic Small Molecule That Can Walk down a Track. *Nat. Chem.* **2010**, *2* (2), 96–101. https://doi.org/10.1038/nchem.481.
(64) Ornes, S. News Feature: What's the Best Way to Build a Molecular Machine? *Proc. Natl. Acad. Sci. U. S. A.* **2018**, *115* (38), 9327–9330. https://doi.org/10.1073/pnas.1811689115.
(65) Bazrafshan, A.; Meyer, T. A.; Su, H.; Brockman, J. M.; Blanchard, A. T.; Piranej, S.; Duan, Y.; Ke, Y.; Salaita, K. Tunable DNA Origami Motors Translocate Ballistically Over Mm Distances at Nm/s Speeds. *Angew Chem Int Ed* **2020**, 8.
(66) Shin, J.-S.; Pierce, N. A. A Synthetic DNA Walker for Molecular Transport. *J. Am. Chem. Soc.* **2004**, *126* (35), 10834–10835. https://doi.org/10.1021/ja047543j.
(67) Fang, J.; Yuan, C.; Li, J.; Li, J.; Yang, T.; Guo, Y.; Wang, D.; Xue, J.; Fu, W.; Xie, G. An Enzyme-Powered, Three-Dimensional Lame DNA Walker. *Biosens. Bioelectron.* **2021**, *177*, 112981. https://doi.org/10.1016/j.bios.2021.112981.
(68) Yehl, K.; Mugler, A.; Vivek, S.; Liu, Y.; Zhang, Y.; Fan, M.; Weeks, E. R.; Salaita, K. High-Speed DNA-Based Rolling Motors Powered by RNase H. *Nat. Nanotechnol.* **2016**, *11* (2), 184–190. https://doi.org/10.1038/nnano.2015.259.
(69) Blanchard, A. T.; Bazrafshan, A. S.; Yi, J.; Eisman, J. T.; Yehl, K. M.; Bian, T.; Mugler, A.; Salaita, K. Highly Polyvalent DNA Motors Generate 100+ PN of Force via Autochemophoresis. *Nano Lett.* **2019**, *19* (10), 6977–6986. https://doi.org/10.1021/acs.nanolett.9b02311.
(70) Yehl, K.; Mugler, A.; Vivek, S.; Liu, Y.; Zhang, Y.; Fan, M.; Weeks, E. R.; Salaita, K. High-Speed DNA-Based Rolling Motors Powered by RNase H. *Nat. Nanotechnol.* **2016**, *11* (2), 184–190. https://doi.org/10.1038/nnano.2015.259.
(71) Piranej, S.; Bazrafshan, A.; Salaita, K. Chemical-to-Mechanical Molecular Computation Using DNA-Based Motors with Onboard Logic. *Nat. Nanotechnol.* **2022**, *17* (5), 514–523. https://doi.org/10.1038/s41565-022-01080-w.
(72) Bazrafshan, A.; Kyriazi, M.-E.; Holt, B. A.; Deng, W.; Piranej, S.; Su, H.; Hu, Y.; El-Sagheer, A. H.; Brown, T.; Kwong, G. A.; Kanaras, A. G.; Salaita, K. DNA Gold Nanoparticle Motors Demonstrate Processive Motion with Bursts of Speed Up to 50 Nm Per Second. *ACS Nano* **2021**, *15* (5), 8427–8438. https://doi.org/10.1021/acsnano.0c10658.

(73) Fjelstrup, S.; Andersen, M. B.; Thomsen, J.; Wang, J.; Stougaard, M.; Pedersen, F. S.; Ho, Y.-P.; Hede, M. S.; Knudsen, B. R. The Effects of Dithiothreitol on DNA. *Sensors* **2017**, *17* (6), 1201. https://doi.org/10.3390/s17061201.